Final Research Performance Report

Federal Agency and Organization: DOE EERE – Geothermal Technologies Program

Recipient Organization: California State University Long Beach
DUNS Number: 006199129
Recipient Address: 1250 Bellflower Blvd., Long Beach, CA 90815

Award Number: DE-EE0002767
Project Title: Recover Act: Verification of Geothermal Tracer Methods in Highly Constrained Field Experiments
Project Period: 1/29/2010-12/31/2012

Principal Investigator: Matthew W. Becker
Professor of Geology
Matt.Becker@csulb.edu
562-985-8983

Report Submitted by: PI
(If other than PI)

Date of Report Submission: May 14, 2014
Reporting Period: [Jan 29, 2010-Sep 30, 2012]
Report Frequency: Quarterly

Project Partners: University of Kansas, Georgios Tsoflias, PI

DOE Project Team: DOE Contracting Officer – Grant Logsdon
DOE Project Officer – Bill Vandermeer

Executive Summary:

The prediction of the geothermal system efficiency is strong linked to the character of the flow system that connects injector and producer wells. If water flow develops channels or "short circuiting" between injection and extraction wells thermal sweep is poor and much of the reservoir is left untapped. The purpose of this project was to understand how channelized flow develops in fracture geothermal reservoirs and how it can be measured in the field. We explored two methods of assessing channelization: hydraulic connectivity tests and tracer tests. These methods were tested at a field site using two verification methods: ground penetrating radar (GPR) images of saline tracer and heat transfer measurements using distributed temperature sensing (DTS).

The field site for these studies is the Altona Flat Fractured Rock Research Site located in northeastern New York State. Altona Flat Rock is an experimental site considered a geologic analog for some geothermal reservoirs given its low matrix porosity. Because soil overburden is thin, it provided unique access to saturated bedrock fractures and the ability image using GPR which does not effectively penetrate most soils. Five boreholes were drilled in a "five spot" pattern covering 100 m^2 and hydraulically isolated in a single bedding plane fracture. This simple system allowed a complete characterization of the fracture. Nine small diameter boreholes were drilled from the surface to just above the fracture to allow the measurement of heat transfer between the fracture and the rock matrix.

The focus of the hydraulic investigation was periodic hydraulic testing. In such tests, rather than pumping or injection in a well at a constant rate, flow is varied to produce an oscillating pressure signal. This pressure signal is sensed in other wells and the attenuation and phase lag between the source and receptor is an indication of hydraulic connection. We found that these tests were much more effective than constant pumping tests in identifying a poorly connected well. As a result, we were able to predict which well pairs would demonstrate channelized flow.

The focus of the tracer investigation was multi-ionic tests. In multi-ionic tests several ionic tracers are injected simultaneously and the detected in a nearby pumping well. The time history of concentration, or breakthrough curve, will show a separation of the tracers. Anionic tracers travel with the water but cationic tracer undergo chemical exchange with cations on the surface of the rock. The degree of separation is indicative of the surface area exposed to the tracer. Consequently, flow channelization will tend to decrease the separation in the breakthrough. Estimation of specific surface area (the ration of fracture surface area to formation volume) is performed through matching the breakthrough curve with a transport model. We found that the tracer estimates of surface area were confirmed the prediction of channelized flow between well pairs produced by the periodic hydraulic tests.

To confirm that the hydraulic and tracer tests were correctly predicting channelize flow, we imaged the flow field using surface GPR. Saline water was injected between the well pairs which produced a change in the amplitude and phase of the reflected radar signal. A map was produced of the migration of saline tracer from these tests which qualitatively confirmed the flow channelization predicted by the hydraulic and tracer tests. The resolution of the GPR was insufficient to quantitatively estimate swept surface area, however. Surface GPR is not

applicable in typical geothermal fields because the penetration depths do not exceed 10's of meters. Nevertheless, the method of using of phase to measure electrical conductivity and the assessment of antennae polarization represent a significant advancement in the field of surface GPR.

The effect of flow character on fracture / rock thermal exchange was evaluated using heated water as a tracer. Water elevated 30 degrees C above the formation water was circulated between two wells pairs. One well pair had been identified in hydraulic and tracer testing as well connected and the other poorly connected. Temperature rise was measured in the adjacent rock matrix using coiled fiber optic cable interrogated for temperature using a DTS. This experimental design produced over 4000 temperature measurements every hour. We found that heat transfer between the fracture and the rock matrix was highly impacted by the character of the flow field. The strongly connected wells which had demonstrated flow channelization produced heat rise in a much more limited area than the more poorly connected wells. In addition, the heat increase followed the natural permeability of the fracture rather than the induced flow field.

The primary findings of this work are (1) even in a single relatively planar fracture, the flow field can be highly heterogeneous and exhibit flow channeling, (2) channeling results from a combination of fracture permeability structure and the induced flow field, and (3) flow channeling leads to reduced heat transfer. Multi-ionic tracers effectively estimate relative surface area but an estimate of ion-exchange coefficients are necessary to provide an absolute measure of specific surface area. Periodic hydraulic tests also proved a relative indicator of connectivity but cannot prove an absolute measure of specific surface area.

Summary of Results by Task:

The primary results of the project are summarized here. The reader is referred to the papers provided in the Appendix for detailed findings and interpretations.

Task 1.0 Hydraulic Tests:

1. **Original Goals**: We hypothesized that the periodic hydraulic testing would provide more sensitivity to the hydraulic connectivity among wells. This was based on findings by other researchers that storativity rather than transmissivity was more indicative of tracer communication. We reasoned that if the test could be kept in a constant state of transition through periodic oscillation of pressure, the observation wells would show connectivity similar to that demonstrated by prior tracer tests and additional tests conducted in Task 2.0.

2. **Actual Accomplishments**: The tests were conducted successfully and as planned. We demonstrated that, as expected, oscillating tests are more indicative of hydraulic connections than pumping tests, at least between closely spaced wells. These experiments and their interpretation are documented in an MS thesis by Eric Guiltinan (now a PhD Student at University of Texas) and presented as a paper at the 2011 Stanford Geothermal Conference (Appendix A) and in a manuscript in review at the Journal of Hydrology (Appendix B).

3. **Variance from Original Goals**: The tests were conducted as planned and confirmed our expected results.

Task 2.0 Tracer Tests:

1. **Original Goals**: Conservative (non-reactive) tracers are commonly used in geothermal fields. The purpose of the conservative tracer tests were to provide an industry standard reference for the hydraulic testing and the reactive tracer tests. The objective of the multi-ionic reactive tests were to demonstrate that effective fracture surface area can be estimated by comparing cationic tracer breakthrough. Diffusive tracers were also proposed as a method for measuring effective surface area.

2. **Actual Accomplishments**: Multi-ionic tracer experiments were conducted in the single bedding plane fracture at the Altona Flat Rock Site in both circulation and single well injection withdraw mode (SWIW). The results of these tests were presented at the 2013 Stanford Geothermal Workshop (Appendix C). By modeling the ionic tracer breakthrough with the program RELAP (in consultation with Paul Reimus, Los Alamos National Laboratory) we found that wells that poorly connected hydraulically created a tracer swept surface area that was 3.8 larger than created by wells that were strongly connected hydraulically. These swept areas were confirmed qualitatively by the GPR imaging (Task 4).

3. **Variance from Original Goals**: Diffusive tests were not used in the field because laboratory tests and think sections demonstrated that the matrix porosity in the sandstone was too small to provide a source of significant diffusive exchange with the fracture. Also, we performed additional experiments in collaboration with PEERi. PEERi had a project under this same program to examine organic tracers (DE-EE00003032). Their field trials with Mt. Princeton Geothermal could not be conducted so they performed field trials at our Altona Flat Rock Site, instead. This work was funded under a subcontract from Mt. Princeton. These results have not yet been published but in Figure 1 we display a CsI breakthrough collected at the site. As is apparent in Figure 1, Cs underwent stronger ion exchange than Li and, therefore, provides greater information regarding swept surface area.

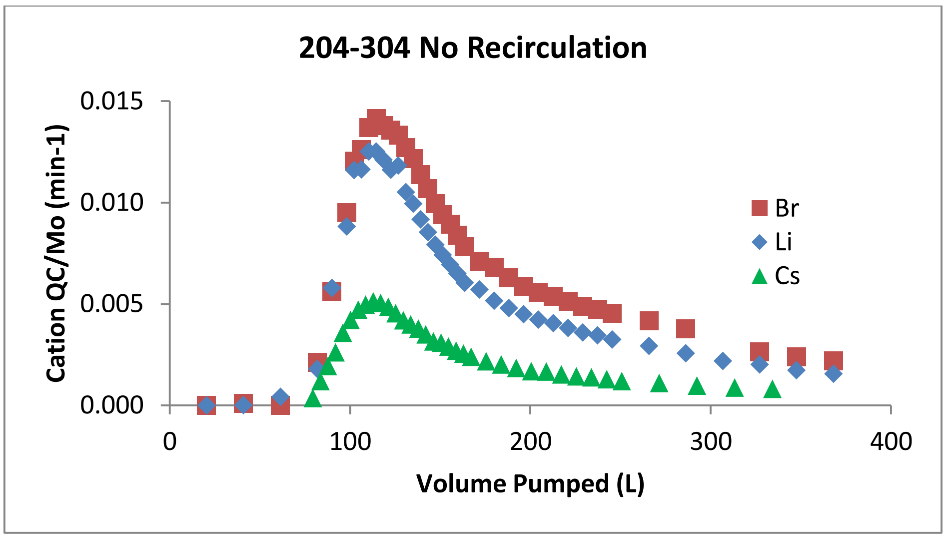

Figure 1. Multi-Cation test conducted at Altona Flat Rock in October, 2012. Cesium proved to be a much more reactive tracer than Lithium and, therefore, better to interrogate the surface area.

Task 3.0 Thermal Tests:

1. **Planned Activities**: The objective of these tests was to measure thermal exchange between a fracture and rock matrix. In geothermal plants cold water is injected and heat extracted from the surrounding rock matrix. As this was not practical in our shallow field experiments, we designed the inverse experiment in which hot water is injected in a relatively cold rock. In this manner we planned to evaluate how sweep efficiency affects heat exchange and how tracer can estimate heat exchange.

2. **Actual Accomplishments**: Thermal experiments were conducted successfully at the Altona Flat Rock Site. Hot water was circulated through the bedrock fracture and heat transfer was measured using a specially constructed fiber optic distributed temperature sensing (FODTS) system. Boreholes were drilled to an elevation just above the fracture and outfitted with coiled fiber optic cable. Coiling the fiber optic cable increased the temperature measurement interval from 1 m to 3 cm.

Results have been published in a thesis by Adam Hawkins (now a PhD student with Jefferson Tester at Cornell) and a paper presented at the 2011 Stanford Geothermal Workshop (Appendix D). The comparison of the heat exchange experiments and GPR imaging is being drafted into a manuscript to be submitted to Geothermics (Figure 2). The manuscript has been delayed due to uncertainties on the GPR imaging (see Task 4).

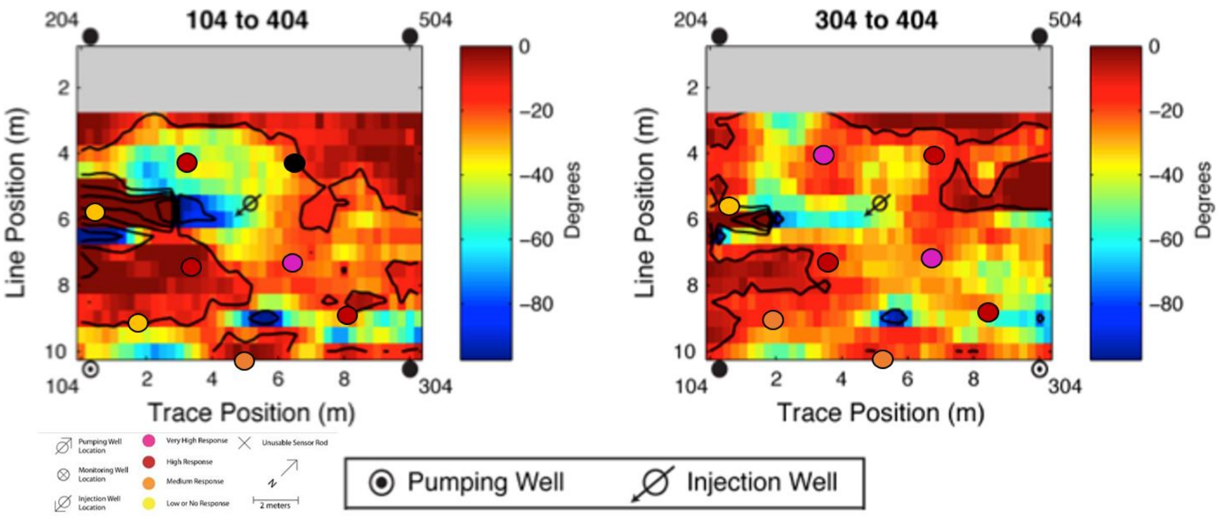

Figure 2. Comparison of heat response in boreholes with phase response of saline tracer circulated between the same wells. Note the strong anisotropy to in the W-E direction that dictates both saline transport and heat transfer. Experimental setup is described in Appendix D.

3. **Variance from Original Goals**: The site was vandalized shortly before the experiments were conducted and two for the FO sensor systems had to be abandoned. We had planned to conduct the heat tracer experiment to all four corner wells but this was not possible due to the missing monitoring points.

Task 4.0 Ground Penetrating Radar (Sub-Contract University of Kansas):

1. **Planned Activities**: Ground Penetrating Radar (GPR) imaging was proposed as a method by which the spatial distribution of tracer and heat exchange could be "ground-truthed". Surface based GPR uses reflected energy from the test fracture (7.6 m depth) to detect the presences of saline tracer and image the variation in fracture aperture. The two-dimensional maps of the fracture provide a comparison to the estimated "sweep" of the fracture by chemical and heat tracer as well as a qualitative comparison to the periodic hydraulic tests of connectivity

2. **Actual Accomplishments**: Imaging of saline tracer was demonstrated by the PI's prior to this project. Through this project, we further established the ability of GPR to image variations in fracture aperture in the absence of saline tracer, i.e. when filled with formation water. To refine this image, the effect of antennae polarization had to be accounted for. This turned out to be a major undertaking the provided unintended additional findings from the project. The effect of polarization was the subject of a M.S.

thesis by KU student Christopher Perll and the results published in an extended abstract to be presented to the 6th International Conference on Environmental and Engineering Geophysics in June of 2014 (Appendix E).

Another important finding of this project is that reflected signal phase is more effective for imaging saline tracer than amplitude. This was predicted in the proposal to the project using theoretical models and was confirmed through field work in the course of the project. These findings were published in a KU M.S. thesis by Matthew Baker and in an extended abstract to the Society of Engineering Geophysics in 2014 (Appendix F).

3. **Variance from Original Goals:** Although the original goals are being met from the project we are well behind schedule. The need to account for polarization and the interpretation of phase, while an important finding, proved to be highly time consuming. In addition, we have been unable to remove sufficient noise from the amplitude maps to provide a reliable basis for inverse modeling (Task 5). The original goal was to invert an aperture field using hydraulic and tracer data and then compare the result to the imaged GPR to verify the reliability of using these data to infer permeability distribution. To date, this has been possible only in a qualitative sense. Former CSULB M.S. student Adam Hawkins, now a PhD student at Cornell continues to work on this problem while PI George Tsoflias continues to work with the GPR data at KU.

Task 5.0 – Modeling and Interpretation

1. **Planned Activities**: Numerical modeling was planned to interpret individual experiments (periodic hydraulic tests, tracer, heat transport) and to integrate datasets and compare them to the GPR images. The objective of this modeling was to quantify the confidence to which hydraulic and tracer breakthrough can anticipate thermal breakthrough.

2. **Actual Accomplishments**: Numerical modeling was conducted successfully for the experiments but, as noted in Task 4, we did not produce an integrative model that could be compared to the GPR. Periodic hydraulic slug tests were interpreted using a previously published method as discussed in the articles presented in Appendix A and B. The model proved effective in deriving transmissivity and storativity from the periodic head data provided discharge could be estimated a priori using water balance calculations. The semi-analytical model RELAP (*Reimus et al.*, 2003) and numerical model MULTRAN (*Sullivan et al.*, 2003) were used in combination to interpret the separation in breakthrough between the anionic and cationic tracers, with a goal of estimating relative surface area to volume ratios in the active fractures in the 104-504 and 204-304 tests (see Appendix C). A one dimensional heat transport solution was used to interpret the thermal breakthrough from the heat tracer experiments as presented in Appendix D.
3. **Variance from Original Goals**: The lack of a single integrative flow and transport model to quantitatively verify hydraulic, tracer, and heat, experiments is disappointing. As discussed in Task 4, it was not possible to complete this task because of uncertainty

and delays in the GPR amplitude and phase responses. Nevertheless, we were able to accomplish our major objectives by modeling the results piecemeal as discussed above.

Summary of Products:

1. Presentations and Publications: A bibliography of presentations and publications resulting from this work is provided below:

   a. Tsoflias G. P., Baker M. and M. Becker (2012), Field GPR monitoring of flow channeling in fractured rock, Abstract NS51B-1834, Fall AGU Meeting, San Francisco, Calif., December 3-7, 2012.
   b. Becker, M.W., K. Remmen, P.W. Reimus, and G.P. Tsoflias (2013), Investigating well connectivity using ionic tracers; PROCEEDINGS, Thirty-Eighth Workshop on Geothermal Reservoir Engineering Stanford University, Stanford, California, February 11-13, 2013, SGP-TR-198.
   c. Hawkins, A.J., M.W. Becker, and G.P. Tsoflias (2012), Field Measurement of Fracture/Matrix Heat Exchange using Fiber Optic Distributed Temperature Sensing, Paper H11A-1152. In American Geophysical Union Fall Meeting, San Francisco, California, December, 2012.
   d. Tsoflias G. P., Perll C., Baker M. and M. Becker (2014), Investigation of Cross-Polarized GPR Signals for Imaging Fracture Flow Channeling, 6th International Conference on Environmental and Engineering Geophysics, Xi'An, China, June 19-22, 2014 (invited).
   e. Perll C. (2013), Evaluating GPR Polarization Effects for Imaging Fracture Channeling and Estimating Fracture Properties, MS Thesis, The University of Kansas, p 157.
   f. Tsoflias G. P., Baker M. and M. Becker (2013), Imaging Fracture Anisotropic Flow Channeling Using GPR Signal Amplitude and Phase, Society of Exploration Geophysicists 83rd Annual Meeting Transactions, Houston, Texas, p. 4428-4433, DOI http://dx.doi.org/10.1190/segam2013-1134.1. (invited)
   g. Tsoflias G. P. and M. W. Becker (2013), Fracture Imaging and Monitoring of Channeled Flow in the Field Using Ground Penetrating Radar, South-Central GSA Meeting, Austin TX, April 4-5, 2013.
   h. Tsoflias G. P., Baker M. and M. Becker (2012), Field GPR Monitoring of Flow Channeling in Fractured Rock, Abstract NS51B-1834, Fall AGU Meeting, San Francisco, Calif., December 3-7, 2012.
   i. Tsoflias G. P., Becker M., Baker M and C. Perll (2012), Advancing Field Methods for GPR Monitoring of Flow Channeling in Fractured Rock, SEG-AGU Hydrogeophysics Joint Workshpop, Boise, Idaho, 8-11 July, 2012.
   j. Tsoflias G. and M. Becker (2012), GPR Characterization of Discrete Fractures and Monitoring of Channeled Flow: Elucidating the Forward Model, 25th Symposium on the Application of Geophysics to Engineering and Environmental Problems (SAGEEP), Tucson, Arizona, March 25-29, 2012. (invited)
   k. Tsoflias G. P., Baker M. and M. W. Becker (2011), Assessing GPR Signal Polarization for 3D Imaging of Fracture Flow Channels, Abstract NS41A-07, Fall AGU Meeting, San Francisco, Calif., December 5-9, 2011.
   l. Tsoflias G. P., Becker M. W. and M. Baker (2011), Monitoring of Flow in Fractured Rock Using Ground Penetrating Radar, National Ground Water

Association Focus Conference on Fractured Rock and Eastern Groundwater Regional Issues, Burlington, Vermont, September 26-27, 2011.

2. Workforce Training: The following students were funded under this project and all graduated with a M.S. Degree.
    a. Krystle Remmen, CSULB, now a Geologist with CH2MHill, Los Angles California
    b. Adam Hawkins, CSULB, now a PhD. Candidate at Cornell University (with J. Tester)
    c. Eric Guiltinan, CSULB, now a Ph.D. candidate at University of Texas at Austin,
    d. Christopher Perll, KU, now…
    e. Matthew Baker, KU, now…

3. Collaborations:
    a. Toward the completion of this project we collaborated with Dr. Yongchun Tang at the Power Environmental Energy Research Institute (PEERi) in Covina California. PEERi had a project under this same program to examine organic tracers (DE-EE00003032). Their field trials with Mt. Princeton Geothermal could not be conducted so they performed field trials at our Altona Flat Rock Site, instead. This work was funded under a subcontract from Mt. Princeton.
    b. We collaborated with Paul Reimus at Los Alamos National Laboratory to interpret the ionic tracer tests. He aided us in using RELAP and MULTRAN to model breakthrough.
    c. Adam Hawkins will continue to work at the Altona Flat Rock Site with Jefferson Tester at Cornell. PI Becker collaborated on a proposal to EERE to continue tracer experiments at the Site.
4. Outreach: A guided field trip was conducted in collaboration with the National Ground Water Association Fractured Rock Conference held in Burlington Vermont, September 26- 27, 2011. Nineteen participants heard talks regarding periodic hydraulic testing, tracer testing, and heat tracer experiments in progress at Altona Flat Rock.
5. Educational Curricula: Experimental results from the project have been incorporated into a hydrogeology course (GEOL 477/577) taught at CSULB. For an example problem, see Appendix G.

Appendix A

Becker, M. W., and E. Guiltinan (2009), Cross-hole periodic hydraulic testing of inter-well connectivity, in *Thirty-Fifth Workshop on Geothermal Reservoir Engineering*, edited, Stanford University, Stanford, California.

PROCEEDINGS, Thirty-Fifth Workshop on Geothermal Reservoir Engineering
Stanford University, Stanford, California, February 1-3, 2010
SGP-TR-188

CROSS-HOLE PERIODIC HYDRAULIC TESTING OF INTER-WELL CONNECTIVITY

Matthew W. Becker, Eric Guiltinan

California State University Long Beach
1250 Bellflower Blvd.
Long Beach, CA 90815 USA
e-mail: mbecker3@csulb.edu

ABSTRACT

Harmonic (periodic) hydraulic tests can establish formation hydraulic properties during active production of geothermal wells. Field experiments were conducted in a fractured sandstone to establish the value of these tests for establishing inter-well connectivity. Sinusoidal head oscillation was induced in well and the propagation of the pressure pulse through a single fracture was measured in four observation wells. Pressure response was interpreted by non-linear regression fitting of the hydraulic diffusion equation to drawdown. Hydraulic diffusivity (transmissivity / storativity) inverted from these tests were found to be much more sensitive to local heterogeneity than traditional constant rate (Theis) tests. The method may be particularly useful for anticipating hydraulic short circuiting in fractured geothermal reservoirs.

INTRODUCTION

Hydraulic connectivity among geothermal wells is a crucial parameter for fluid circulation: too poor of a hydraulic connection leads to insufficient circulation rates between injectors and producers and too strong of a connection leads to hydraulic short-circuiting and inefficient heat transfer. The establishment of hydraulic connectivity is even more important in Enhanced Geothermal Systems (EGS) where permeable fractures are artificially created in an otherwise impermeability rock. In EGS reservoirs, poor connectivity may mean zero circulation.

The importance hydraulic connectivity has led to the use of chemical tracers for formation evaluation. Tracers have been shown to be quite effective in establishing hydraulic connections among wells [*Chrysikopoulos*, 1993; *Rose et al.*, 2001; *Shook*, 2001]. However, tracer tests typically last weeks or more and may incur expensive analytic costs. In addition, tracer selection must be tailored to the specific geochemical and thermodynamic conditions in the reservoir to avoid degradation or adsorption of the tracer in the reservoir [*Chrysikopoulos*, 1993].

Hydraulic communication between wells are better characterized using tracer tests than standard hydraulic tests because the latter are relatively insensitive to local changes in permeability [e.g. *Butler and Liu*, 1993; *Oliver*, 1993]. This is particularly true when a Cooper-Jacob analysis is used because the late time drawdown data are emphasized. *Meier et al.* [1998] showed that late-time drawdown is largely independent of position of the monitoring well. Some researchers have improved upon the spatial resolution of hydraulic transmissivity by inverting cross-hole tests among multiple boreholes [*Li et al.*, 2007]. Although these methods have demonstrated some success in shallow environments, the large number of wells necessary for such inversions is not available in geothermal fields.

Transmissivity and storativity are difficult to decouple in hydraulic testing. For example, numerical synthetic pumping tests conducted in heterogeneous transmissivity fields result in an overestimation of storativity variability caused as a result of the transmissivity variability [*Meier et al.*, 1999; *Meier et al.*, 2001]. Thus, some researchers have looked to the ratio of T/S, or the hydraulic diffusivity (D) as an indicator of hydraulic conductivity. *Knudby and Carrera* [2006] used Monte Carlo simulations of a hypothetical two-dimensional aquifer to show that hydraulic diffusivity was a reasonable indicator of tracer connectivity among wells. Traditional constant rate tests, on the other hand, were shown to be poor predictors of both tracer and hydraulic communication.

In this article we explore the use of harmonic hydraulic testing to measure hydraulic connectivity. Harmonic testing involves the variation of head and/or discharge rate in a periodic manner. Harmonic testing dates back to the 1970's in the petroleum field where it is used to establish formation characteristics [*Hollaender et al.*, 2002]. More recently it has been applied to at least one geothermal field [*Nakao et al.*, 2005]. The practical advantage of the harmonic test is that production or injection need only be varied, not stopped. The practical disadvantage is that tests generally need to be run longer than a constant-rate test to detect distant boundaries [*Hollaender et al.*, 2002].

We performed harmonic testing in a well-characterized sandstone formation in New York State, USA. Hydraulic experiments were conducted among wells isolated in a single fracture within a 100 m^2 area. Head was varied in the source well in a sinusoidal manner. The results of harmonic tests are compared here to constant-rate (Theis) tests among the same wells.

METHODS

Field Site

Field tests were conducted at the Altona Flat Rock experimental site . Altona Flat Rock is part of a large system of Cambrian Potsdam Sandstone (well-sorted quartzose) pavements that were stripped of overburden during the last glaciation and remain exposed today [*Rayburn et al.*, 2005]. There are laterally extensive sub-horizontal (dipping ~3º) bedding plane partitions visible in numerous outcrops surrounding the site. Because the sandstone is highly cemented with silica, primary porosity is insignificant in comparison to secondary porosity. Extensive tracer experiments have been conducted among five 15-cm-diameter open-hole wells arranged in a 5-spot configuration with 10 meters on a side. The wells intersect a major sub-horizontal fracture 7.6 meters below ground surface that has been the focus of those investigations. The thin overburden has been cleared in this area to present a clean sandstone pavement for GPR imaging of the 7.6 m fracture. The Altona Flat Rock site is part of the William H. Miner Agricultural Research Institute which has granted us permission to develop the site and has provided us with logistical support.

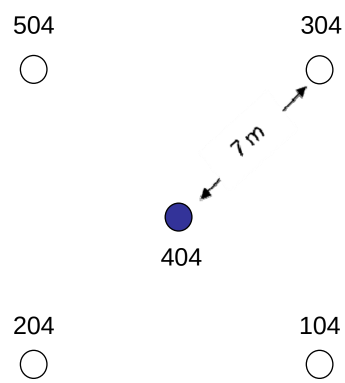

Figure 1: Well field configuration at the Altona Flat Rock Site.

Harmonic Testing

Harmonic testing was conducted by oscillating a solid cylinder or slug in and out of Well 404 while recording head variations in the surrounding wells (*Figure 1*). All wells were isolated to the single bedding plane fracture at 7.6 m depth using inflatable packers in the 15 cm diameter boreholes. Head was disturbed in Well 404 by raising and lowering the slug in a sinusoidal manner using a winch driven by a computer-controlled stepping motor (*Figure 2*). Head could be precisely controlled using this system but discharge could not be measured independently. Head in the disturbed well and the surrounding monitoring wells was monitored using pressure transducers (Druck) read by a datalogger (Campbell Scientific).

Constant Rate Testing

Constant rate tests were conducted by pumping Well 404 with a Grundfos Rediflo2 pump at a rate of 4.2 lpm and monitoring drawdown in the surrounding wells using pressure transducers (Druck) connected to a datalogger (Campbell Scientific). Transmissivity and storativity were determined by curve fitting a Theis well function (completely confined infinite extent) to the drawdown for each of the monitoring wells. It should be noted that the constant rate tests are not entirely comparable to the harmonic tests because only the pumping well was isolated by packers in the constant rate tests. Consequently, in the constant rate tests monitoring wells may be more affected by well bore storage.

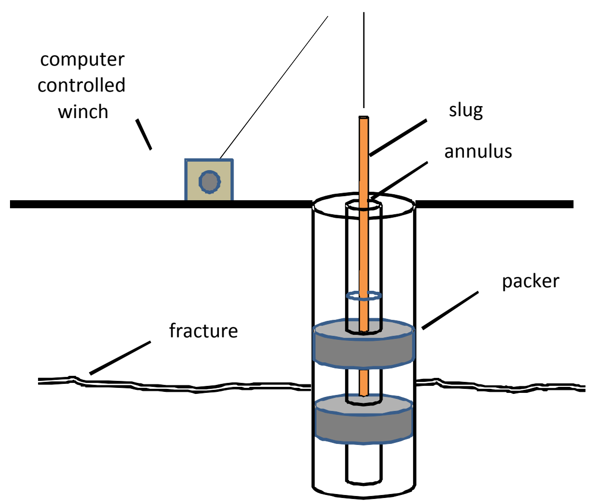

Figure 2: Well field configuration at the Altona Flat Rock Site.

RESULTS

An example of the head variation in the disturbed well (404) and the monitoring wells is shown in *Figure 3*. Note that the head is disturbed in Well 404 by only about 6 cm. Pressure scatter at maximum drawdown is due to water running off the slug as is raised from the water.

The wells show a highly varying pressure response to the oscillation of the slug in Well 404. Well 204 responds with almost no attenuation of amplitude or phase lag. Wells 304 and 504 show a moderate attenuation of amplitude and an evident phase lag. Well 104 shows a highly dampened response to the oscillation in Well 404 but it is also influenced by a longer period pressure boundary. This long wavelength influence does not correlate with barometric pressure. Wind-driven fluctuation in the level of a nearby surface water body is one feasible explanation but we have not yet explained satisfactorily the behavior.

Because discharge was not measured in these tests, it is impossible to decouple T and S from hydraulic diffusivity [*Renner and Messar*, 2006]. To determine hydraulic diffusivity we fit the hydraulic diffusion equation to the drawdown data. The formation acts as a transfer function affecting the propagation of the pressure pulses in the disturbed well. The analysis is completed in Laplace space and inverted numerically. In this manner, convolution of the impulse function and the transfer function is accomplished through multiplication in the Laplace domain. The sinusoidal input function that describes the perturbation of head from the initial level is

$$\bar{\delta}_s = p_0\left(\frac{\omega}{s^2+\omega^2}\right)\exp\left(\frac{\theta s}{\omega}\right) \qquad (1)$$

where p_0 is the amplitude of the pressure disturbance in the input well, ω is the frequency of the disturbance, θ is the phase shift from reference time, and s is the Laplace variable. The formation transfer function is

$$\bar{\delta}_f = \frac{K_0\left(r\sqrt{\frac{s}{D}}\right)}{K_0\left(r_w\sqrt{\frac{s}{D}}\right)} \qquad (2)$$

where K_0 is the Bessel Function, r is the radial distance to the observation well, r_w is the radius of the disturbed well, and D is the hydraulic diffusivity. The total response at the observation well is then

$$\bar{\delta}_t = \bar{\delta}_s \cdot \bar{\delta}_f\,. \qquad (3)$$

Equation 3 is inverted to the time domain numerically [*Becker and Charbeneau*, 2000].

We fit *Equation 3* to observed head oscillations in all four observation wells for four different sinusoid

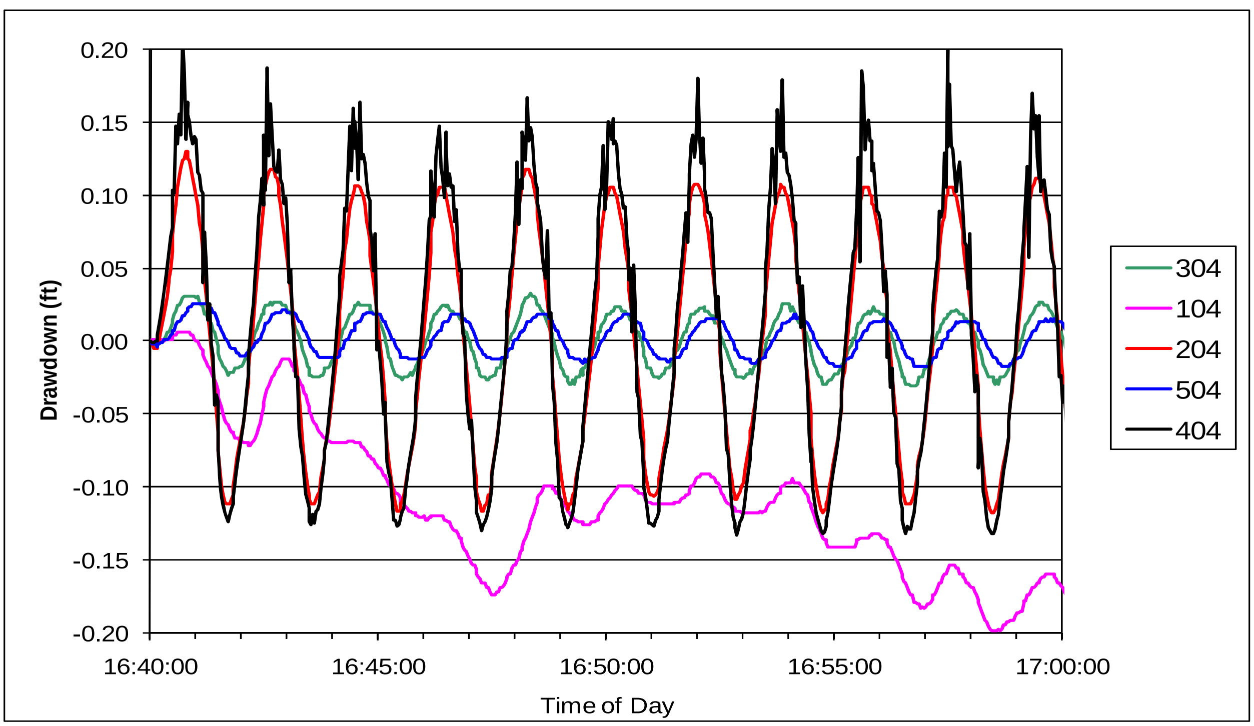

Figure 3: Example harmonic test for a 113 second period of oscillation. Well 404 was the disturbed well.

periods. *Figure 3* show an example fit to the data. First the input signal is fit with a sinusoid function (1) then the observation well data are fit by varying hydraulic diffusivity (2). Best fit hydraulic diffusivity is determined though a Levenberg-Marquardt non-linear regression.

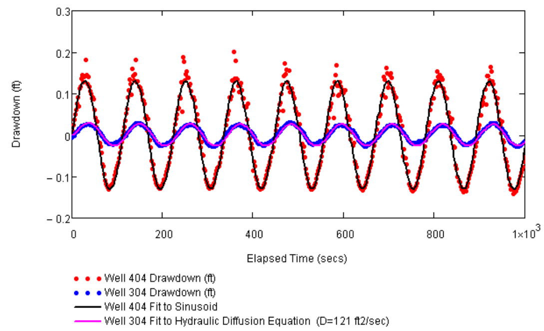

Figure 4. Fit of sinusoid (1) to drawdown in disturbed Well 404 and hydraulic diffusion equation (3) to drawdown in observation Well 304.

The model derived hydraulic diffusivity for wells 304 and 504 are show in *Figure 5*. Note that diffusivity decreases as a power law with increasing period. The decrease in hydraulic diffusivity implies a decrease in transmissivity or increase in storativity with period. We consider a variation in storativity to be more likely. The use of storativity implies that water is removed or added to storage as a linear function of head. This is not necessarily the case in a fractured formation where elastic storage is a function of rock stiffness. The expansion and contraction of a fracture is not likely to be a linear function of pressure in realistic systems [*Cappa et al.*, 2006].

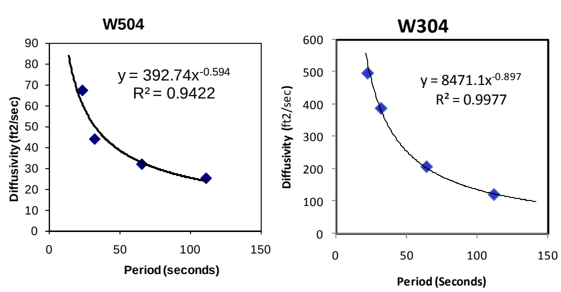

Figure 5. Variation in estimated hydraulic diffusivity with period.

Nakao et al. [2005] saw a similar relationship between the separation in time of pressure pulses and derived hydraulic diffusivity in a Sumikawa Geothermal Field in Japan. They attributed this relationship to the fractured nature of the reservoir and used the relative contribution of matrix and fracture storage to derive fracture spacing. In our case, however, we work in only a single fracture and the primary matrix permeability is essentially negligible. *Renner and Messar* [2006] conducted periodic tests in a fractured sandstone and observed a decrease in hydraulic diffusivity with increasing period. They attributed this behavior to the channelized nature of flow in a fracture. Water moves primarily through a "backbone" of channels with storage of water in smaller aperture regions. Longer harmonic periods, they conjecture, allow for more water exchange with these tighter regions and, consequently, a larger effective storativity and smaller hydraulic diffusivity. We are presently comparing multiple conceptual models to interpret the data.

Well 204 also demonstrates a general decrease in diffusivity with period but the trend is not regular as in Well 304 and 504. We attribute the poor trend to the highly connected nature of Well 204 with Well 404, which makes model fitting problematic. Hydraulic diffusivity inverted from model fits to the hydraulic response range between 10^{15} to 10^{19} ft^2/sec. This is more than 13 orders-of-magnitude greater than hydraulic diffusivities determined from Wells 304 and 504. At these diffusivities Darcy's Law may not be valid. Well 104 is not interpreted here due to the long wavelength influence on the heads that were alluded to previously.

Finally, we compare the hydraulic diffusivity determined through these harmonic tests to those derived through a Theis well function fitting of constant rate drawdown tests. *Figure 6* shows the drawdown versus log-time plot for a test in which Well 404 was pumped at 4.2 lpm [*Talley*, 2005].

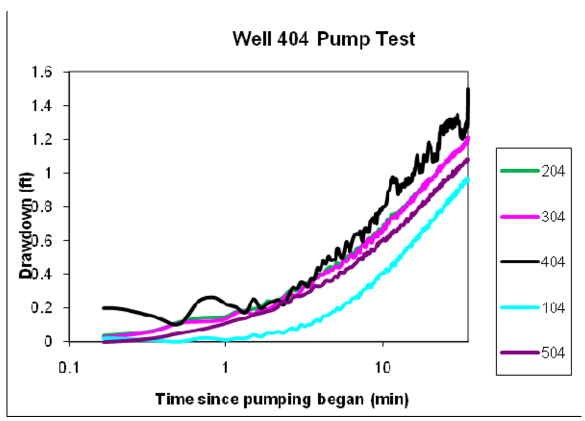

Figure 6. Drawdown from a constant rate pumping tests conducted in the same wells in which the harmonic tests were conducted.

In agreement with the harmonic tests, Well 104 shows a poor hydraulic connection to Well 404. Also in agreement with the constant rate tests, the harmonic tests show a very good connection between

Well 204 and 404. There is a slight discrepancy between the two methods, however, in that Well 304 and 204 behave very similarly in the constant rate test, while 304 and 504 behave similarly in the harmonic tests (*Figure 3*).

The hydraulic diffusivities derived from fitting of the standard Theis equation to the constant rate tests are shown in *Table 1*. Hydraulic diffusivities determined from the harmonic test vary over a much greater range than those determined from the constant rate test. Constant rate tests produce hydraulic diffusivities that are within 5% for Well 304 and 504, for example, while the harmonic tests produce estimates that differ by about an order-of-magnitude between the wells.

Table 1: Hydraulic parameters derived from constant rate tests.

Well	T (ft^2/s)	S	D (ft^2/s)
204	4.9E-04	2.3E-04	2.18
104	4.4E-04	4.6E-04	0.97
304	4.7E-04	2.4E-04	1.91
504	5.1E-04	2.8E-04	1.81

CONCLUSIONS

The practical advantages of periodic hydraulic tests are well known and have been exploited in the petroleum industry for decades. Periodic tests do not require an additional net withdrawal or injection of fluid so they can be conducted without cessation of operations. In geothermal fields, this means injection or pumping rates can be varied in a periodic manner to determine hydraulic properties, even after wells are put into production. Such post-completion information can be valuable for well infilling.

There is a potential advantage in periodic tests beyond the purely practical. The harmonic hydraulic tests conducted here by oscillating a slug in a bedrock well showed greater sensitivity to formation heterogeneity than more traditional constant-rate (Theis) tests. All four monitoring wells showed distinctly different responses in the harmonic tests while only one well was obviously less connected as interpreted from the constant rate tests.

Harmonic tests may provide information regarding scaling of heterogeneous hydraulic properties. Although interpretation varies, harmonic tests in this fractured formation and at least two others [*Nakao et al.*, 2005; *Renner and Messar*, 2006] show a decrease in hydraulic diffusivity with increasing period of pressure pulsing. This result deserves more attention as it may provide a method by which the channelization of flow may be quantified in geothermal fields. Channelization or "short-circuiting" of flow has important implications for heat transfer in geothermal reservoirs.

ACKNOWLEDGEMENTS

This research was funded by grants from the Department of Energy Environmental Remediation Sciences Program (DE-SE0001778) and Geothermal Technologies Program (DE-EE0002767). The authors are grateful for the continuing support provided by David Franzi at SUNY Plattsburgh and the William H. Miner Agricultural Research Institute.

REFERENCES

Becker, M. W., and R. J. Charbeneau (2000), First-passage-time transfer functions for groundwater tracer tests conducted in radially convergent flow, *Journal of Contaminant Hydrology*, *45*(4), 361-372.
Butler, J. J., and W. Z. Liu (1993), Pumping Tests in Nonuniform Aquifers - the Radially Asymmetric Case, *Water Resources Research*, *29*(2), 259-269.
Cappa, F., Y. Guglielmi, J. Rutqvist, C. F. Tsang, and A. Thoraval (2006), Hydromechanical modelling of pulse tests that measure fluid pressure and fracture normal displacement at the Coaraze Laboratory site, France, *Int J Rock Mech Min*, *43*(7), 1062-1082.
Chrysikopoulos, C. V. (1993), Artificial Tracers for Geothermal Reservoir Studies, *Environmental Geology*, *22*(1), 60-70.
Hollaender, F., P. S. Hammond, and A. C. Gringarten (2002), Harmonic Testing for Continuous Well and Reservoir Monitoring, Paper SPE 77692 presented at SPE Annual Technical Conference and Exhibition, 29 September-2 October 2002, San Antonio, Texas edited, Society of Petroleum Engineers.
Knudby, C., and J. Carrera (2006), On the use of apparent hydraulic diffusivity as an indicator of connectivity, *Journal of Hydrology*, *329*(3-4), 377-389.
Li, W., A. Englert, O. A. Cirpka, J. Vanderborght, and H. Vereecken (2007), Two-dimensional characterization of hydraulic heterogeneity by multiple pumping tests, *Water Resources Research*, *43*(4).
Meier, P. M., J. Carrera, and X. Sanchez-Vila (1998), An evaluation of Jacob's method for the interpretation of pumping tests in heterogeneous formations, *Water Resources Research*, *34*(5), 1011-1025.
Meier, P. M., J. Carrera, and X. Sanchez-Vila (1999), A numerical study on the relationship between transmissivity and specific capacity in heterogeneous aquifers, *Ground Water*, *37*(4), 611-617.
Meier, P. M., A. Medina, and J. Carrera (2001), Geostatistical inversion of cross-hole pumping tests for identifying preferential flow channels within a shear zone, *Ground Water*, *39*(1), 10-17.

Nakao, S., T. Ishido, K. Hatakeyama, and K. Ariki (2005), Analysis of Pulse Tests in a Fractured Geothermal Reservoir: Case Study at the Sumikawa Field in Japan, Proceedings World Geothermal Congress, Antalya, Turkey, 24-29 April 2005.

Oliver, D. S. (1993), The influence of nonuniform transmissivyt and storativity on drawdown, *Water Resources Research*, *29*(1), 169-178.

Rayburn, J. A., P. L. K. Knuepfer, and D. A. Franzi (2005), A series of large, Late Wisconsinan meltwater floods through the Champlain and Hudson Valleys, New York State, USA, *Quaternary Science Reviews*, *24*(22), 2410-2419.

Renner, J., and M. Messar (2006), Periodic pumping tests, *Geophys J Int*, *167*(1), 479-493.

Rose, P. E., W. R. Benoit, and P. M. Kilbourn (2001), The application of the polyaromatic sulfonates as tracers in geothermal reservoirs, *Geothermics*, *30*(6), 617-640.

Shook, G. M. (2001), Predicting thermal breakthrough in heterogeneous media from tracer tests, *Geothermics*, *30*(6), 573-589.

Talley, J. (2005), Imaging channelized flow in fractured rock using surface GPR, Master of Science thesis, University at Buffalo, Buffalo.

Appendix B

Guiltinan, E., and M. W. Becker (submitted), Measuring Well Hydraulic Connectivity in Fractured Bedrock using Periodic Slug Tests, *J. Hydrol.*.

Measuring Well Hydraulic Connectivity in Fractured Bedrock using Periodic Slug Tests

Eric Guiltinan[1] and Matthew W. Becker, Department of Geological Sciences, California State University Long Beach, Long Beach, California, USA

Abstract:

Periodic hydraulic tomography experiments were conducted in a five-spot well cluster completed in a single bedding plane fracture. Periodic aquifer tests were performed by using a slug to create a periodic head disturbance in one well and observing the phase shift and attenuation of the head response in a monitoring well. Transmissivity (T) and storativity (S) were inverted independently from the frequency spectrum of head response. Inverted T decreased and S increased with oscillation period. Estimated S was more variable among well pairs than T, suggesting S may be a better estimator of hydraulic connectivity among closely spaced wells. Periodic slug tests produce more variable estimates of transmissivity and storativity than a constant rate test conducted in the same wells. Periodic slug tests appear to be a practical and effective technique for establishing local scale spatial variability in hydraulic parameters.

1.0 Introduction

Flow channelization has long been recognized as a hallmark of groundwater flow in fractured bedrock systems [*Tsang and Neretnieks*, 1998]. The physical nature of the problem is described simply through the "local cubic law" which dictates that water flow rate is related cubically to the local fracture aperture. Prediction of flow in a natural bedrock system is not so simple, however, as the distribution of aperture and its interaction with water flow is highly variable even within a single fracture. Understanding flow in bedrock consequently requires site specific hydraulic characterization to be conducted.

[1] Corresponding author, Eric Guiltinan, now at the University of Texas, Austin
email: eric.guiltinan@utexas.edu

Typical pumping and slug test configurations are not well suited to bedrock environments. Because of the small water storage in bedrock, the hydraulic radius of influence of a pumping well extends rapidly outward implying that only the earliest drawdown contains local information. Early drawdown is often dominated by well-bore storage and formation damage effects in open boreholes. Slug test responses are weighted more toward local hydraulics but are even more sensitive to borehole influences.

A periodic hydraulic test potentially overcomes these limitations of pumping and slug tests. Periodic (also called harmonic, oscillatory, or sinusoidal) tests are conducted by creating an oscillating head in one well and observing the corresponding oscillatory head response in one or more observation wells. Because the head signal is in a constant state of transience, periodic tests highlight the influence of formation storativity on drawdown response. The repeatability of the transience allow initial effects of well bore storage and pump priming to be isolated. Most interestingly, periodic tests are capable of interrogating different portions of the formation without the addition of observations wells. This is because the spatial weighting of hydraulic response to hydraulic conductivity (K) and storativity (S) is sensitive to the frequency of the head oscillation [*Cardiff et al.*, 2013; *Renner and Messar*, 2006]. By repeating a periodic hydraulic test at varying frequency, different regions of the formation can be tested for hydraulic conductivity and storativity. While this is true for any type of groundwater system, it is particularly effective in bedrock systems because the small formation water volume means a small head perturbation propagates far from the test well.

Periodic hydraulic testing is by no means a new measurement technique. Periodic hydraulic testing was used in the oil industry as early as 1966 [*Black and Kipp*, 1981]. During the 1970s it was put to use in oil production wells using alternating periods of flow and shut-in [*Hollaender* *et al.*, 2002]. The earliest report of periodic tests in the groundwater literature regards the use of naturally occurring periodic oscillations such as earth tides or barometric changes [*Black and Kipp*, 1981]. These natural periodic influences have the advantage of extending over many kilometers but do not indicate inter-well connectivity [*Rasmussen et al.*, 2003].

We demonstrate here the use of periodic testing in a single bedding plane fracture at the 10 m scale. In our experiments, head is varied in the test well by oscillating a slug up and down at the level of water in the well. The periodic head response is observed at four observation wells. Because we limit our experiment to a single fracture we highlight aperture variability rather than fracture network connectivity in our experiments. Matrix porosity is negligible so the hydraulics are dictated by the fracture only.

The development of this characterization tool is particularly relevant to geologic fluid circulation systems such as those used in groundwater remediation, petroleum recovery, and geothermal plants. In all of these systems flow channeling can lead to a short circuiting of the circulation system that may result in inefficient extraction of contaminated groundwater, petroleum reserves, or geothermal heat, respectively. Periodic tests may provide a means for characterizing problematic channeling either before or during operations. Because it is not necessary to extract water or shut down pumps to conduct these tests, they are likely to be much more cost effective than shut-in hydraulic or cross-hole tracer tests.

2.0 Methods

<u>2.1 Experimental Site</u>

The Altona Flat Rock Site is located in Clinton County, New York, approximately 25 km northwest of Plattsburgh, New York. It is situated in an exposed pavement of the Cambrian aged

Potsdam formation, laid bare by a glacial dam burst at the end of the most recent glacial advance [*Rayburn et al.*, 2007]. The upper Potsdam is highly cemented with silica and thin sections from the site reveal local matrix porosity that is around 1 to 2 percent. Consequently, fractures are the dominant conduit for flow with insignificant flow and storage in the matrix at local scales.

Ground penetrating radar testing revealed a major water-bearing bedding plane fracture (dipping ~3°) at 7.6 m below ground surface [*Becker and Tsoflias*, 2010; *Jennifer Talley*, 2005; *J. Talley et al.*, 2005; *Tsoflias and Becker*, 2008]. A well field was installed at the site in a “five spot” configuration in 2004 (Figure 1).

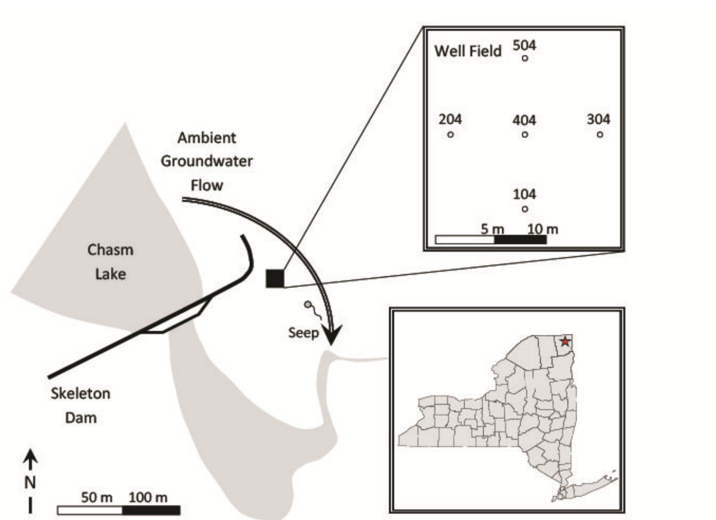

Figure 1. Site well configuration.

2.2 Periodic Hydraulic Testing

To create the sinusoidal head signal in the hydraulic source well, a “slug” consisting of a 1.9 cm diameter watertight cylinder was lifted and lowered via a winch operated by a computer controlled stepper motor (Driver: ST10-Si, Motor: HT34-486, Applied Motion Products, Watsonville, CA). A straddle packer system (specially constructed of PVC by RocTest, Lakewood, Colorado) with a 10.2 cm (4 in) inner diameter was used to isolate the hydraulic disturbance to the target fracture. Figure 2 depicts the field set up for the source well during the tests. To observe the head response in the source and monitoring wells (104, 205, 304, 504), pressure transducers (Druck 1230 Series and a Solinst Levelogger model #3001) were installed. The transducers in the monitoring wells were placed within straddle packers (Vanderlans and Sons, Lodi, California) and routed to a datalogger (CR1000, Campbell Scientific, Logan, Utah) allowing the transducers to be monitored in real-time. Three different frequencies were created at each well while all were monitored for head.

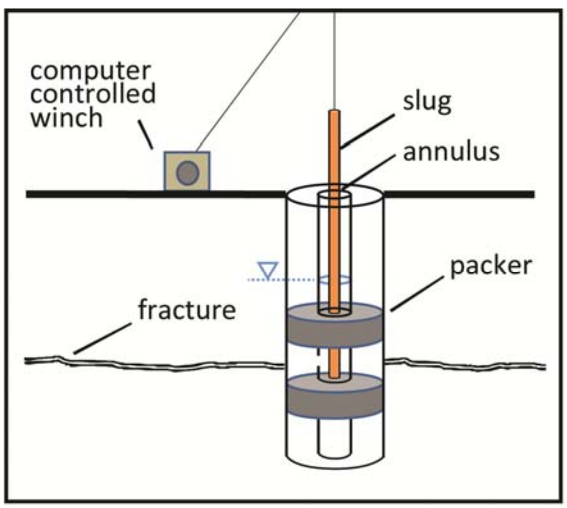

Figure 2. Schematic of the experimental design of the hydraulic source well.

Interpretation was performed by assuming confined conditions and a formation of infinite extent. The boundary value problem is then

$$\frac{\partial^2 s}{\partial r^2} + \frac{1\partial s}{r\partial r} = \frac{1}{D}\frac{\partial s}{D\partial t} \tag{1}$$

$$s(r,0) = 0 \qquad (2)$$

$$s(\infty,t) = 0 \qquad (3)$$

$$\lim_{r\to 0} r\frac{\partial s}{\partial r} = -\frac{Q}{2\pi T} \qquad (4)$$

where s is the observed drawdown, r is the distance from the center of the pumping well, T is the formation transmissivity, and D is the hydraulic diffusivity. The hydraulic diffusivity is the ratio of the transmissivity to the storativity (D = T/S). The flux of water from the well, Q, is the complex periodic function:

$$Q(t) = Q_0 e^{i\omega t} \qquad (5)$$

where i is the complex variable and w is the frequency of the oscillation.

As presented by Rasmussen et al., [2003] the solution for drawdown is

$$s(r,t) = \frac{Q}{2\pi T} K_0\left(r\sqrt{\frac{i\omega}{D}} \right) \qquad (6)$$

where K_0 is the zero-order modified Bessel function of the second kind . Equation (6) neglects a period of early time in which the signal has not yet become steady. The amplitude of the drawdown oscillation in an observation well is

$$|s| = \frac{Q}{2\pi T}\left| K_0\left(r\sqrt{\frac{i\omega}{D}} \right) \right| \qquad (7)$$

And the phase shift between the flux at the test well and the drawdown at the observation well is

$$\phi_0 = \phi_s - \phi_Q = \arg\left\{K_0\left(r\sqrt{\frac{i\omega}{D}}\right)\right\} \tag{8}$$

Where ϕ_s is the phase of the drawdown signal and ϕ_Q is the phase of the flux of water at the test well.

Following Rasmussen et al., [2003], parameters T and D (and therefore S = T/D) were obtained by fitting periodic functions to the measured flux and drawdown data. At the test well, the oscillating flux is fit with the cosine function

$$Q(t) = Q_0 e^{i\omega t} = Q_0 \cos(\omega t - \phi_Q) = Q_1 \cos \omega t + Q_2 \sin \omega t \tag{9}$$

where Q_0 is the amplitude, ω the frequency, and ϕ_Q this phase of the of the flux signal at the test well. The coefficients Q_1 and Q_2 represent $Q_0 \cos\phi_Q$ and $Q_0 \sin\phi_Q$, respectively. Likewise, the drawdown at the observation well is fit with the function

$$s(t) = s_1 \cos \omega t + s_2 \sin \omega t \tag{10}$$

where the coefficients s_1 and s_2 represent $s_0 \cos\phi_s$ and $s_0 \sin\phi_s$, respectively, and s_0 is the amplitude of the drawdown. After fitting the functions (9) and (10) to the flux and drawdown signals, respectively, the phase lag, ϕ_0, is found from

$$\phi_0 = \arctan\left(\frac{s_2}{s_1}\right) - \arctan\left(\frac{Q_2}{Q_1}\right) \tag{11}$$

The magnitude of the drawdown, s_0, is found by normalizing the modulus of the drawdown signal to the modulus of the flux signal as

$$s_0 = \frac{|s|}{|Q|} = \frac{\sqrt{s_1^2 + s_2^2}}{\sqrt{Q_1^2 + Q_2^2}} \quad . \tag{12}$$

To facilitate the inversion of D from ϕ_0 in equation 8, we use fifth order logarithmic polynomial [*Rasmussen et al.*, 2003]:

$$\ln(\frac{\omega r^2}{D}) = \sum_{c=0}^{5} c_i \left(\ln \phi_0\right)^i \tag{13}$$

where c_i = (-0.12665, 2.8642, -0.47779, 0.16586, -0.076402, 0.03089). Transmissivity is obtained by solving (7) for transmissivity and substituting (12):

$$T = \frac{\left| K_0\left(r\sqrt{\frac{i\omega}{D}} \right) \right|}{2\pi s_0} \tag{14}$$

To determine flux in and out of the test well due to the oscillation of the slug (9), the volume of water gained or lost from the test well must be calculated from the slug displacement and water rise and fall in the well. The slug displacement was controlled through programed movements in the stepper motor and the water level in the well was measured with a pressure transducer. The difference between slug displacement and the water level change was fit to a sinusoidal signal

$$V(t) = Q_0 \sin\left(\frac{2\pi t}{T_0} \right) \tag{15}$$

where T_0 is the period of the oscillating water level. The derivative of Equation 15 with respect to time is, therefore, the flow rate into and out of the fracture:

$$Q(t) = Q_0 \left(\frac{2\pi}{T_0} \right) \cos\left(\frac{2\pi t}{T_0} - \phi_Q \right) \tag{16}$$

The process of extracting the flux is illustrated for well 404 in Figure 3. The flow rate precedes the observed change in head by a slight phase shift [*Renner and Messar*, 2006].

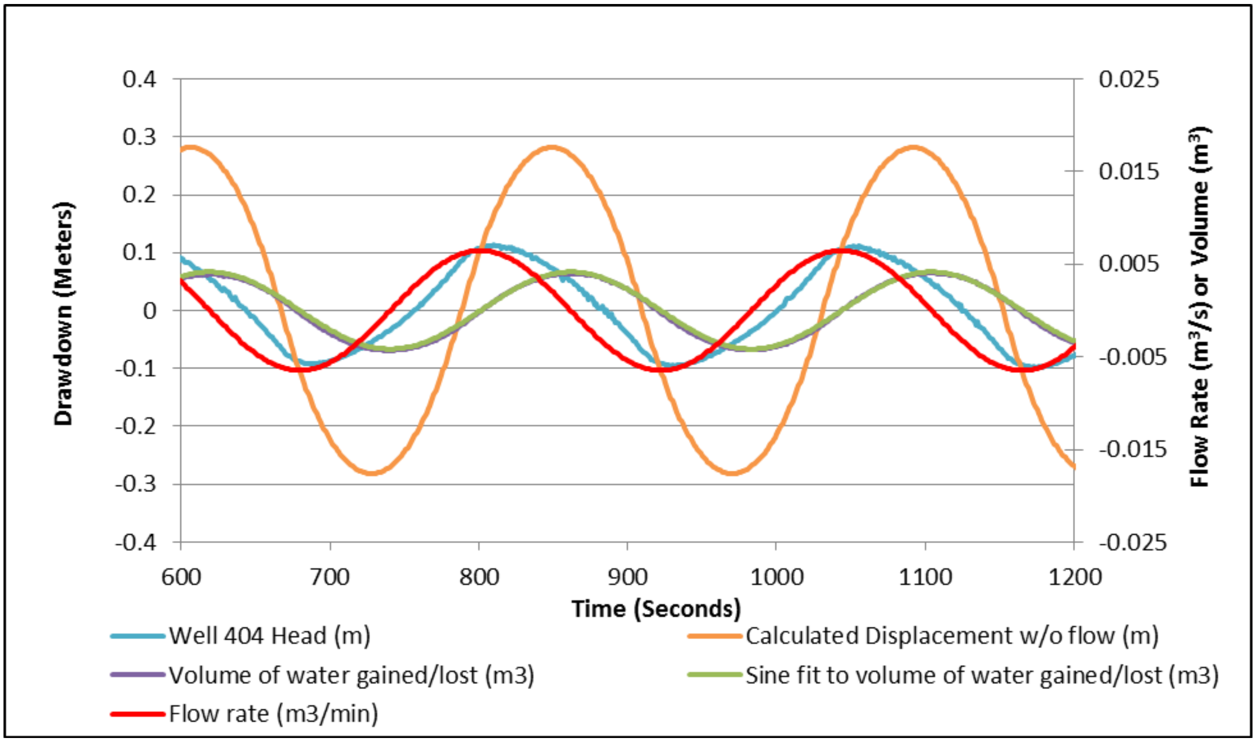

Figure 3. An example of the extraction of flow in and out of the test well: well 404 with a slug oscillation period of 242.6 seconds.

2.3 Constant Rate Pumping Test

A constant-rate pump test was conducted as a comparison to the periodic slug tests. A submersible pump was used to withdraw water at a 3.3 L/min from the isolated fracture in well 404. Straddle packers were installed across the target fracture in each monitoring well and pressure transducers (Leveloggers, Solinst, Waterloo, Canada) were deployed to monitor the drawdown.

3 Results

3.1 Periodic Hydraulic Tests

Figures 4, 5, and 6 show the head response in wells equidistant from the test well, 404, at the three different slug oscillation periods. Head response in the monitoring wells differs from the test well in both amplitude and phase. Well 204 displays a very slight attenuation of the amplitude and minor phase lag, while well 104 shows a significant attenuation and phase lag. Wells 304 and 504 show a nearly identical response in between that of 204 and 104. The relationships between the signals are independent of the frequency of the test; however, the amplitude increases with decreasing period as the displaced water has less time to enter the formation. The amplitudes range from about 0.1 to 0.2 meters. The greatest attenuation and phase lag of the input signal was observed at well 104. Past experience with slug, and tracer testing at the site confirm that this well is poorly connected hydraulically to the remainder of the well field [*Becker and Tsoflias*, 2010; *J. Talley et al.*, 2005].

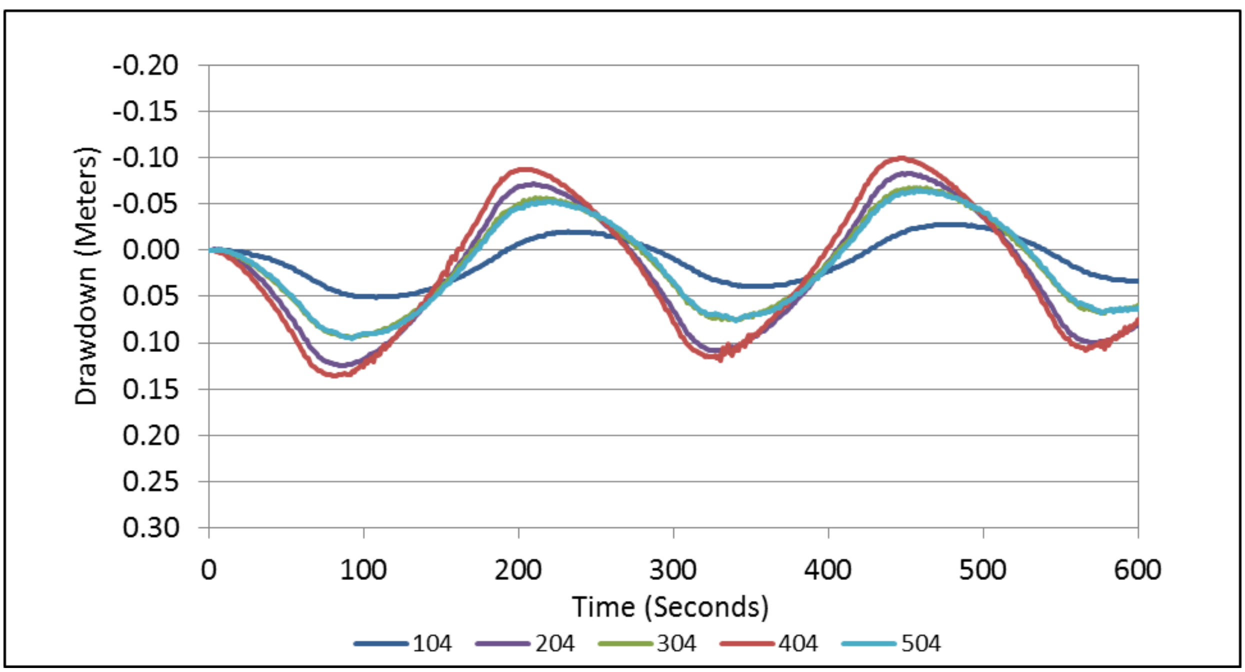

Figure 4. Periodic test at well 404. Period – 242.6 seconds.

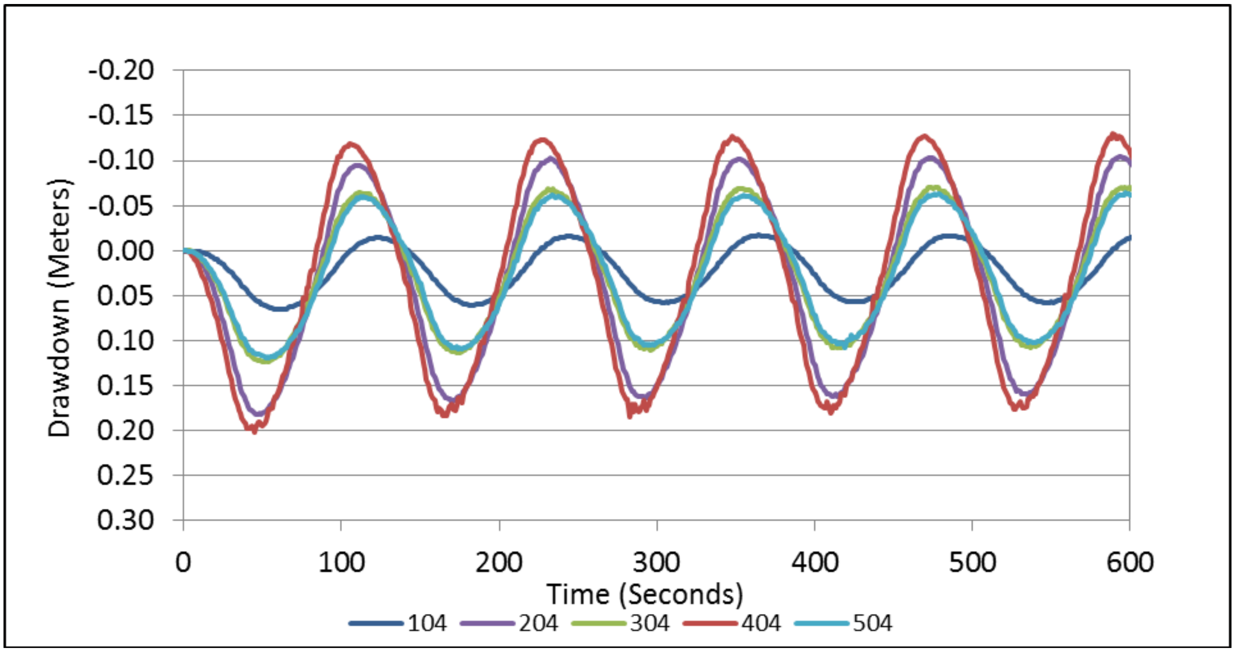

Figure 5. Periodic test at well 404. Period - 121.4 seconds.

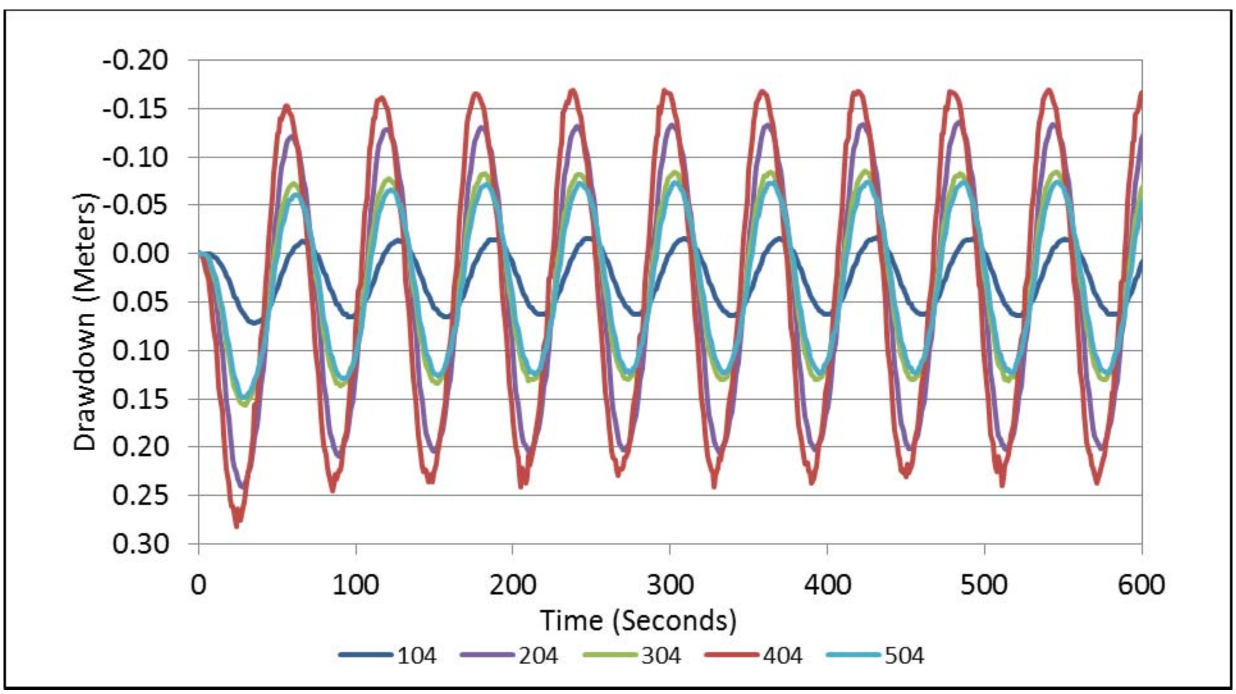

Figure 6. Periodic test at well 404. Period – 60.7 seconds.

The result of using well 104 as the test well is shown in Figure 7. The experimental setup was as describe previously, except that the straddle system and slug was moved from well 404 to 104. Well 404 was fitted with the same straddle system used in the other observation wells. As expected, the poor hydraulic communication between well 104 and the remainder of the well field results in a highly attenuated and shifted periodic response in all of the monitoring wells.

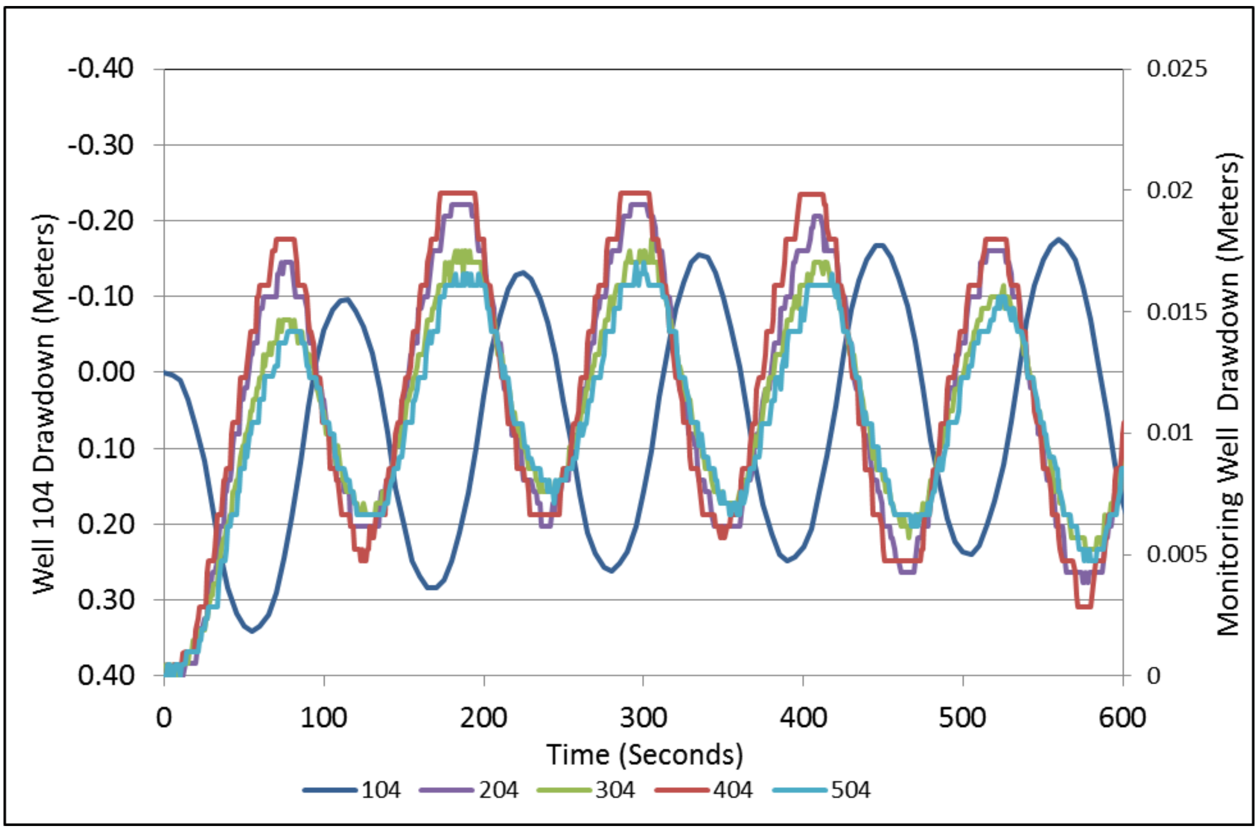

Figure 7. Periodic test at well 104. Period – 112.4 seconds.

Figure 8 presents all estimates of hydraulic diffusivity based upon responses to head oscillations in well 404. The estimates of hydraulic diffusivity range over two orders-of-magnitude among well pairs. Well 204 had the greatest estimated hydraulic diffusivity and 104 the smallest. The hydraulic diffusivity estimates for all tests are presented in Table 1.

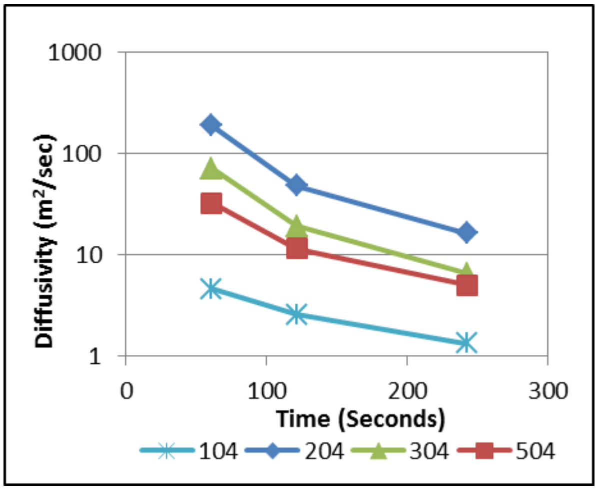

Figure 8. Calculated hydraulic diffusivity during the well 404 tests.

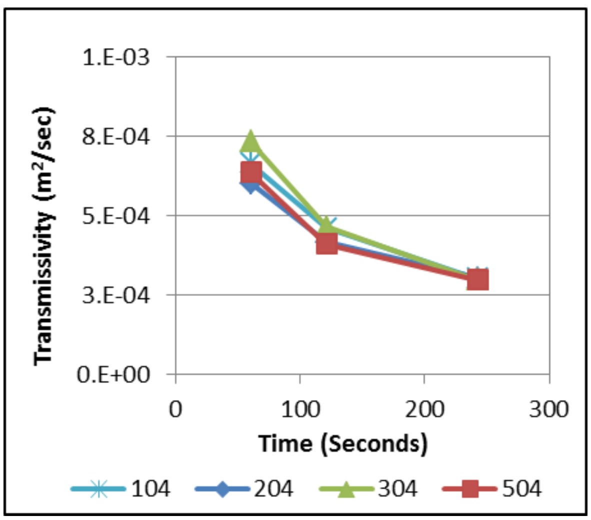

Figure 9. Calculated transmissivity from the well 404 tests.

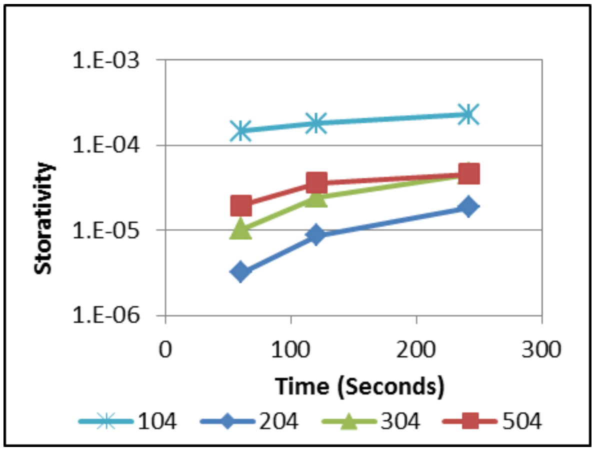

Figure 10. Calculated storativity from the well 404 tests.

Tested Well	Period (seconds)	Hydraulic Diffusivity Estimated at Observation Well (m^2/s)				
		104	204	304	404	504
104	56.2	--	9.85	8.51	6.99	11.56
	112.4	--	3.58	2.88	2.13	4.58
	242.6	--	0.96	0.79	0.52	1.43
204	60.7	4.17	--	39.67	22.15	15.24
	121.4	4.20	--	50.32	48.75	17.72
	242.6	2.01	--	14.65	10.87	6.29
304	56.2	9.26	168.15	--	106.62	152.81
	112.4	5.20	67.60	--	30.61	37.39
	224.6	2.23	18.58	--	6.72	8.88
404	60.7	4.59	189.75	71.49	--	32.34
	121.4	2.59	48.18	19.05	--	11.49
	242.6	1.34	16.45	6.57	--	4.99
504	56.2	15.24	56.84	166.32	58.65	--
	112.4	7.00	17.35	29.55	12.40	--

	224.6	3.68	7.47	10.29	5.06	--

Table 1. Estimates of hydraulic diffusivity obtained from periodic tests conducted in the Altona well field.

3.2. Constant Rate Test

An example of the drawdown response to constant pumping of well 404 is shown in Figure 11. For comparison, a fitted Theis curve is shown as a solid line. The early time deviation suggests that the formation is likely due to a negative skin effect (local increase in hydraulic conductivity) resulting from borehole damage. Drawdown observed at the other three wells (204, 304, 504) also show similar deviation at early time.

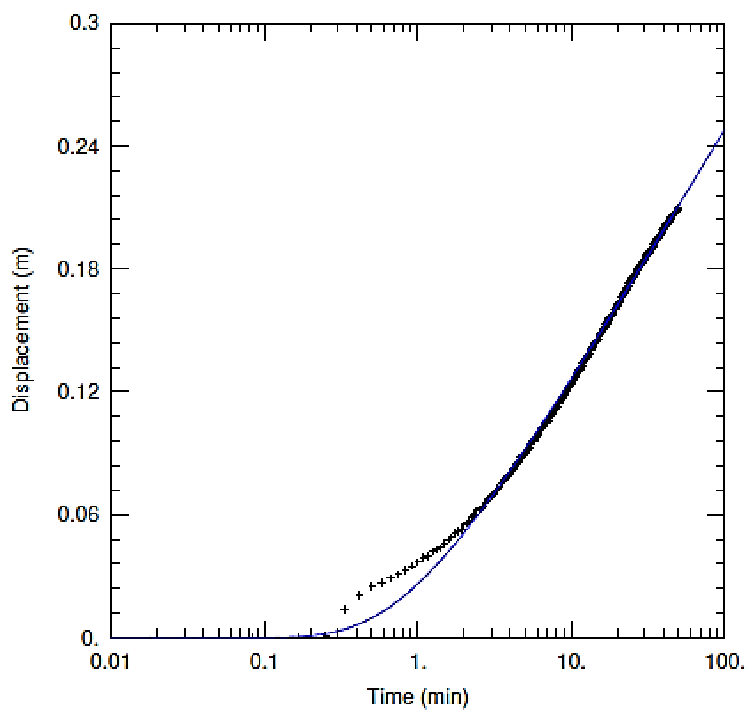

Figure 11. Drawdown (points) at well 104 in response to pumping well 404. A Theis drawdown curve is displayed for comparison (solid line; T = 8.2 E-5 m^2/sec; S = 2.2 E-4).

Hydraulic diffusivity was determined for all four observation wells by fitting a Theis curve to the drawdown, ignoring the first few minutes of drawdown. Figure 12 is a comparison of the hydraulic diffusivity estimates derived from the periodic and the constant rate tests. Note that the variability in estimates from the periodic tests is much greater than that from the constant rate tests.

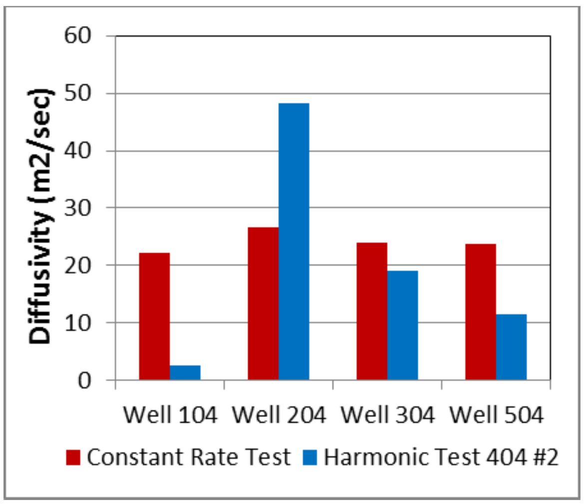

Figure 12. A comparison of hydraulic diffusivity estimates from the constant rate test and periodic test at well 404.

4. Discussion

Estimates of hydraulic diffusivity obtained from the periodic tests (Figure 8) vary by more than an order of magnitude even though all measurements were made in the same bedding plane fracture. The range in hydraulic diffusivity is due primarily to the variation in estimated storativity (Figure 10) rather than transmissivity (Figure 9). Prior theoretical studies have shown that storativity tends to be the dominant control on hydraulic connection among closely spaced wells and may also be a strong predictor of tracer transport [*Knudby and Carrera*, 2006].

Periodic test estimates of hydraulic diffusivity decreased as oscillation period increased for all monitoring wells. *Renner and Messar* [2006] observed a similar relationship in sinusoidal periodic hydraulic tests conducted in fractured sandstone bedrock. In their tests, wells were hydraulically connected through a series of fractures, rather than a single fracture. These authors suggested that estimated storativity increased with oscillation period as water had more time to exchange between a "backbone" of more direct water flow and the surrounding fracture void space.

Cardiff et al. [2013] arrived at a different interpretation of *Renner and Messar's* [2006] experiments using numerical simulations of periodic hydraulic tests. They used adjoint methods to show that the sensitivity of observed drawdown to the hydraulic diffusivity changes spatially as period changes. The relationship between oscillation period and estimates of hydraulic diffusivity results from the particular arrangement of the hydraulic diffusivity field. It is interesting to note, however, that in all of our tests, and those of *Renner and Messar* [2006], hydraulic diffusivity estimates decreased with increasing period. A consistent trend is not explained by sensitivity to the diffusivity field alone. Furthermore, the comparison of transmissivity and storativity by *Cardiff et al.* [2013] was performed in a homogenous flow field with only small perturbations of hydraulic parameters to establish sensitivity. It is possible that a similar analysis conducted in a highly heterogeneous flow field may predict the "backbone" of flow conjectured by *Renner and Messar* [2006]. At higher oscillation frequencies *Cardiff et al.* [2013] found enhanced sensitivity to interwell hydraulic parameters, which could be interpreted as a flow channel in heterogeneous media.

A common estimate of the range of impact from a hydraulic test in a confined formation is the hydraulic radius or, in the case of oscillatory tests, penetration depth. Both are given by, or proportional to, $1.5\sqrt{D\tau}$, where τ is the characteristic time of penetration (e.g. [*Renner and Messar*, 2006]). In periodic tests, τ is assumed to be the period of oscillation while in constant rate tests τ is taken to be the time since pumping began. In our tests, period of oscillation was between 1 and 4 minutes, while the pumping test was conducted over a period of 10's of minutes or more. This suggests that pumping tests interrogated a much larger area than the periodic tests.

Because transmissivity is derived from the late time slope of the pumping test drawdown, the lack of sensitivity to well position in pumping tests is expected. Estimates of storativity are more sensitive to early drawdown but, as previously noted, may be masked by borehole skin in our tests. The radius of influence (depth of penetration) for periodic tests ranged between 4 m and 161 m with an average of 61 m (calculated from Table 1). These measures suggest that even the periodic tests influenced an area much larger than the well field. In retrospect, we should have run our experiments at shorter periods (0.5 to 4 min) to focus on interwell distances.

It is important to note that none of the analyses mentioned thus far account hydromechanical dilation of the fracture aperture. Decreasing the period of head oscillation provides less time for water to move into the formation resulting in larger amplitude waves with greater hydraulic force to dilate fractures. This could explain the decrease in transmissivity with period shown in figure 10. Other researchers have performed single well experiments in which aperture dilation has been measured by extensiometers in response to repeated slug testing [*Svenson et al.*, 2008]. The use of coupled extensiometer measurements perhaps in concert with tilt meter measurements [*Vasco et al.*, 2001], would help constrain the interpretation of periodic testing in bedrock.

4.2 Conclusions

Periodic hydraulic experiments were conducted by oscillating a slug in a wellbore isolated at a saturated bedrock fracture. A periodic solution of the standard Theis problem was used to extract transmissivity and storativity from observed amplitude and phase relationships between the tested well and an observation well. Storativity estimates, and to a lesser extent transmissivity estimates, varied distinctly among some well pairs in the five tested wells. The ratio of estimated transmissivity to estimated storativity (hydraulic diffusivity) has been suggested as a predictor of hydraulic and transport connectivity in heterogeneous groundwater systems [*Knudby and Carrera*, 2006]. The connectivity estimated in these periodic hydraulic tests corresponds to tracer experiments and ground penetrating radar imaging conducted in the same well field (e.g. [*Becker and Tsoflias*, 2010]).

For problems that require local estimations of hydraulic connectivity among wells, periodic slug tests appear to be an attractive tool. Aside from the localization of the hydraulic stress field, they require no net extraction of water. A mass neutral test is beneficial in contaminated environments where extracted water must be tested and/or treated. Advances in the sensitivity of pressure transducers and the fact that only precision and not accuracy is required to interpret periodic tests, suggest that they may be useful in near well porous as well as fractured bedrock systems. A clean oscillating signal with a slug connected to a computer controlled winch is relatively straightforward and produces excellent signal to noise ratio of head perturbations.

Consequently, it may be worth considering periodic slug tests in closely spaced wells completed in formations of small storativity.

Periodic tests were repeated for oscillation periods that varied between one and four minutes. Thus measured, the apparent transmissivity decreased and the storativity increased with oscillation period. Past researchers have observed this same relationship from periodic pumping tests in fractured bedrock and interpreted it as a result of flow interaction between a "backbone" of flow in channels and surrounding stagnant zones [*Renner and Messar*, 2006]. A relationship between oscillation period and estimated hydraulic transmissivity has been observed also in single pulse tests [*Nakao et al.*, 2005].

More recent synthetic simulations [*Cardiff et al.*, 2013] show that varying source periodicity changes the sensitivity of head oscillations in observation wells to distributed hydraulic parameters, suggesting our observations may be the result of structured heterogeneity (e.g. open apertures or cross-cutting fractures) in the vicinity of the well field. This analysis may turn out to be a generalization of the "backbone" conceptualization of flow. Not considered in these analyses or our own is that hydromechanical effects can cause non-linear relationships between head and storage [*Cappa et al.*, 2008; *Rutqvist and Stephansson*, 2003; *Svenson et al.*, 2008].

For comparison, a constant rate pumping test was conducted in the same well field and analyzed by fitting a Theis curve to the drawdown. Hydraulic diffusivity estimated from each of the four observation well responses varied much less than those estimated from the periodic tests at all oscillation periods. Periodic tests appear to be much more sensitive to the hydraulic connectivity among well pairs. The trend in hydraulic diffusivity estimated from periodic tests with increasing oscillation periods did not approach that estimated from the steady rate tests, as might be expected [*Cardiff et al.*, 2013].

Research to date, including this work, suggests that the period-dependency of apparent (i.e. homogenous equivalent) hydraulic parameters is a result of heterogeneous flow and storage to the well. Thus, periodic hydraulic testing may provide a means to characterizing flow channeling in bedrock fractures and fracture networks. In our estimation, the full potential of periodic testing for bedrock is as of yet untapped due to a lack of theoretical understanding. To date, theoretical models have been based upon near homogeneous hydraulic parameters and/or linear hydromechanical properties, while fractured bedrock rarely exhibits either quality in response to hydraulic stresses. Given the impact of flow channeling on groundwater, geothermal, and petroleum problems, the use of periodic hydraulic tests in bedrock systems deserves further investigation.

Acknowledgements:

This work was funded by the Department of Energy Geothermal Technologies Program (DE-EE0002767) and Office of Biological and Environmental Research (ER64856-1034288-0015367). We gratefully acknowledge support of the Miner Agricultural Research Institute and Drs. David Franzi and Edwin Romanowicz of SUNY Plattsburgh.

References:

Becker, M. W., and G. P. Tsoflias (2010), Comparing Flux-Averaged and Resident Concentration in a Fractured Bedrock using GPR, *Wat. Resour. Res.*, *46*, W09518, doi: 09510.01029/02009WR008260.
Black, J. H., and K. L. Kipp (1981), Determination of hydrogeological parameters using sinusoidal pressure tests; a theoretical appraisal, *Water Resources Research*, *17*(3), 686-692.
Cappa, F., Y. Guglielmi, J. Rutqvist, C. F. Tsang, and A. Thoraval (2008), Estimation of fracture flow parameters through numerical analysis of hydromechanical pressure pulses, *Water Resources Research*, *44*(11).

Cardiff, M., T. Bakhos, P. K. Kitanidis, and W. Barrash (2013), Aquifer heterogeneity characterization with oscillatory pumping: Sensitivity analysis and imaging potential, *Water Resources Research*, n/a-n/a.

Hollaender, F., P. S. Hammond, and A. C. Gringarten (2002), Harmonic Testing for Continuous Well and Reservoir Monitoring, in *SPE Annual Technical Conference and Exhibition*, edited, Society of Petroleum Engineers, San Antonio, Texas.

Knudby, C., and J. Carrera (2006), On the use of apparent hydraulic diffusivity as an indicator of connectivity, *Journal of Hydrology*, *329*(3-4), 377-389.

Nakao, S., T. Ishido, K. Hatakeyama, and K. Ariki (2005), Analysis of Pulse Tests in a Fractured Geothermal Reservoir-Case Study at the Sumikawa Field in Japan, in *Proceedings World Geothermal Congress, Antalya, Turkey, 24-29 April 2005*, edited.

Rasmussen, T. C., K. G. Haborak, and M. H. Young (2003), Estimating aquifer hydraulic properties using sinusoidal pumping at the Savannah River site, South Carolina, USA, *Hydrogeology Journal*, *11*(4), 466-482.

Rayburn, J. A., D. A. Franzi, and P. L. K. Knuepfer (2007), Evidence from the Lake Champlain Valley for a later onset of the Champlain Sea and implications for late glacial meltwater routing to the North Atlantic, *Palaeogeography Palaeoclimatology Palaeoecology*, *246*(1), 62-74.

Renner, J., and M. Messar (2006), Periodic pumping tests, *Geophys J Int*, *167*(1), 479-493.

Rutqvist, J., and O. Stephansson (2003), The role of hydromechanical coupling in fractured rock engineering, *Hydrogeology Journal*, *11*(1), 7-40.

Svenson, E., T. Schweisinger, and L. C. Murdoch (2008), Field evaluation of the hydromechanical behavior of flat-lying fractures during slug tests, *Journal of Hydrology*, *359*(1-2), 30-45.

Talley, J. (2005), Imaging channelized flow in fractured rock using surface GPR, Altona, NY, New York State University at Buffalo, Buffalo.

Talley, J., G. S. Baker, M. W. Becker, and N. Beyrle (2005), Four dimensional mapping of tracer channelization in subhorizontal bedrock fractures using surface ground penetrating radar, *Geophys. Res. Lett.*, *32* (doi:10.1029/2004GL021974).

Tsang, C. F., and I. Neretnieks (1998), Flow channeling in heterogeneous fractured rocks, *Reviews of Geophysics*, *36*(2), 275-298.

Tsoflias, G. P., and M. W. Becker (2008), Ground-penetrating-radar response to fracture-fluid salinity: Why lower frequencies are favorable for resolving salinity changes, *Geophysics*, *73*(5), J25-J30.

Vasco, D. W., K. Karasaki, and K. Kishida (2001), A coupled inversion of pressure and surface displacement, *Water Resources Research*, *37*(12), 3071-3089.

Appendix C

Becker, M. W., K. Remmen, P. W. Reimus, and G. P. Tsoflias (2013), Investigating well connectivity using ionic tracers; PROCEEDINGS, *Thirty-Eighth Workshop on Geothermal Reservoir Engineering*, Stanford University, Stanford, California, February 11-13, 2013, SGP-TR-198.

PROCEEDINGS, Thirty-Eighth Workshop on Geothermal Reservoir Engineering
Stanford University, Stanford, California, February 11-13, 2013
SGP-TR-198

INVESTIGATING WELL CONNECTIVITY USING IONIC TRACERS

Matthew W. Becker and Krystle Remmen
California State University, Long Beach, Geology Department
1250 Bellflower Boulevard
Long Beach, California, 90840, USA
matt.becker@csulb.edu

Paul W. Reimus
Los Alamos National Laboratory
P.O. Box 1663, MS J966
Los Alamos, NM 87545

Georgios P. Tsoflias
2The University of Kansas,
1475 Jayhawk Blvd.,
Lawrence, KS 66045

ABSTRACT

Fluid circulation in geothermal reservoirs is often impacted by an uneven sweep of water between injection and pumping wells. Poor sweep efficiency may lead to poor fluid circulation or, at the opposite extreme, flow short-circuiting and premature thermal breakthrough at an extraction well. Multiple ionic tracer tests have been proposed as one method by which reservoir conformance issues may be identified. Herein are reported the results of inter-well tracer tests conducted at the Altona Flatrock Fractured Bedrock experimental site during the Summer of 2011. Lithium was used as a reactive tracer and bromide the non-reactive tracer (verified with deuterium oxide). Separation between cation and anion tracers in the breakthrough was minimal except in cases where tracer was circulated between wells with poor hydraulic connection. Numerical modeling of the breakthrough curves indicates that the swept surface area to volume ratio was about 4 times greater between wells with poor hydraulic connection than between those with strong hydraulic connection. Ground penetrating radar images of saline fluid circulated between the same wells confirms that a weaker hydraulic connection results in a more extensive flow sweep of the fracture. This relationship is likely enhanced in fracture networks, suggesting that strong hydraulic connection among geothermal circulation may not result in strong heat extraction as a result of poor sweep efficiency.

INTRODUCTION

The efficiency of multiwall geothermal systems is dependent up the swept surface area of the hot rock mass. In fractured bedrock system, this equates to the fracture surface area that is encountered by fluid circulated among wells. Estimating this surface area has been a goal of tracer testing for many years. Over 100 tests have been conducted in geothermal reservoirs [*Shook and Forsmann*, 2005]. The vast majority of these tests have utilized conservative (non-reactive) tracers to measure residence time among well pairs. Recent efforts have been toward "smart" tracers which can provide more detailed characterization of fractures, including surface area [*Tester and others*, 2006].

One method for interrogating surface are in geothermal reservoirs is to compare the breakthrough of anionic and cationic species in a forced gradient tracer experiment [*Dean et al.*, 2012]. The concept is that cationic tracers will undergo exchange with cations on fracture surfaces, while anionic tracers will be non-reactive in the same system. The separation in breakthrough curves can, therefore, be attributed to the availability of exchangeable cations on the rock surface and the surface area available for exchange.
It is difficult to estimate the cation exchange capacity (CEC) of the rock surface independently from the tracer experiment. Obtaining representative cores of fracture surfaces is challenging because mineral surfaces are chemically altered in the presence of

flowin geothermal fluids, and flow fields are not homogeneous. Even so, ionic tracers tests can be useful in a relative sense. For example, assuming that the CEC of the rock surface does not change before and after stimulation, ionic tracers can provide an estimate of the relative increase in surface area due to stimulation. Furthermore, assuming that the CEC does not vary appreciably throughout a fractured geothermal reservoir, ionic tracers can provide an estimate of the relative surface area swept by fluid flowing between different well pairs. It is this latter application that is investigated in the experiments described here.

Cation exchange reactions may be expressed as

$$A + BX \rightarrow AX + B \quad (1a)$$
$$2A + CX_2 \rightarrow 2AX + C \quad (1b)$$
$$2B + CX_2 \rightarrow 2BX + C \quad (1c)$$

where A and B are monovalent cations and C is a divalent cation [*Dean et al.*, 2012]. X is a negatively charged surface site. Equation 1 shows that a monovalent cation can exchange either with monovalent or divalent cations on mineral surfaces.

Ionic tracer experiments have been utilized in studies of diffusive exchange between fractures and matrix [*Becker and Shapiro*, 2003; *Callahan et al.*, 2000; *Reimus and Callahan*, 2007] and as analogs for radionuclide transport [*Reimus et al.*, 2003]. Ionic tracers in non-porous rock have also shown strong separation with relative capacity for ion exchange [*Andersson et al.*, 2002]. Column tests with rock samples from Fenton Hill indicated that lithium and Cesium were particularly promising ions for use in geothermal tracer studies [*Dean et al.*, 2012].

FIELD SITE

The field site is located in the Altona Flat Rocks, in northern New York, USA about 4 miles northwest of West Chazy, New York. The Altona Flat Rocks region is highly unique in the Northeastern United States, because a glacial flood stripped soil overburden off of bedrock, exposing an expanse of sandstone with shallow groundwater in bedrock fractures [*Rayburn et al.*, 2005]. The relevant formation, the Cambrian-aged Potsdam Sandstone is well cemented with silica and as a consequence has effective porosities of less than 1 percent. Ubiquitous fracturing, however, makes the formation highly permeable and it is used as an aquifer for drinking water supply.

The experiments were conducted in the William Miner Experimental Forest, which is managed by the William H. Miner Agricultural Institute (http://www.whminer.com/). The experimental site was selected due to its lack of soil cover, the shallow water levels, and the presence of strong sub-horizontal bedding plane fracturing. Reconnaissance ground penetrating radar located a reflection at 7.6 m deep that was interpreted to be an open bedding plane fracture. Subsequent drilling of a well field confirmed the location of a permeable fracture that was suitable for conducting tracer and hydraulic testing. Since the drilling of the wells in 2004, multiple experiments have been carried out at the site to investigate flow, solute transport, and heat exchange in fractured bedrock [*Becker and Tsoflias*, 2010; *Castagna et al.*, 2011; *Guiltinan and Becker*, 2010; *Hawkins and Becker*, 2012; *Talley et al.*, 2005; *Tsoflias and Becker*, 2008].

The well field is located near an abandoned dam (Skeleton Dam) that creates a strong hydraulic gradient across the well field as water flow from the created reservoir (Chasm Lake) to a small ledge which produces a seepage face (Figure 1). A five-spot 15 cm diameter well pattern penetrates a conductive sub-horizontal fracture 7.6 m meters below the surface. Transmissivity of the fracture is estimated to be about 5 m^2/day which suggests a mean hydraulic aperture of about 0.5 mm based upon the local cubic law [*Talley et al.*, 2005]. For all experiments, the target bedding plane fracture was isolated with inflatable packers such that we could work in essentially an single sub-horizontal flow field.

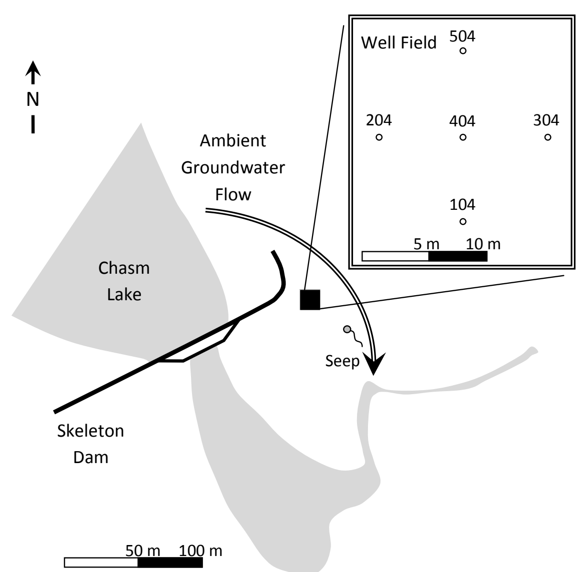

Figure 1: Map of the field area and well field (inset).

The groundwater at Altona Flat Rocks is very low in dissolved solids. Typical background electrical conductivity can be less than 100 mS/m. ICP-MS cation analyses of background water pumped from the fracture yielded high levels of iron (1440 ppb), and confirmed that calcium (Ca2+), sodium (Na+), magnesium (Mg2+), and potassium (K+) are the dominant cations present in solution. Both lithium (Li+) and bromide (Br -) have very low to nonexistent background concentrations, often less than 1 ppm. The Potsdam bedrock fractures present a quartz rich mineral surface in clean breaks but show iron staining in the presence of flowing water. Ion exchange in the field site, therefore, is likely dominated by secondary mineral coatings on the fracture surface that have yet to be fully characterized. Based upon diffusion cell tests conducted over the period of months, matrix diffusion is negligible at the hour time scales over which these experiments were conducted.

TRACER EXPERIMENTS

Lithium and bromide were used at the ionic tracers of choice in the experiments discussed here. Tracer injection solutions were created by dissolving LiBr into extracted groundwater. Tracers were detected in the field using ion specific electrode and samples returned to the laboratory were analyzed using ion chromotraphy (IC). IC analyses are reported here.

Tracer experiments were conducted under forced gradient in a "full-dipole" configuration between well pairs. For the full dipole test, water is pumped from the extraction well at the same rate it is introduced at the injection well. Before water is returned to the formation it passes through a mixing tank at which tracer can be introduced the recirculating system and breakthrough can be measured at the pumping well (Figure 2). Because tracer is recirculated through the system, breakthrough demonstrates multiple concentration peaks due to the recirculation of the initial injection of tracer. However, since the volume in the full mixed tank is known, breakthrough curves may be modeled using transport equations that account for the convolution of transfer functions representing storage in the mixing tank, boreholes, and formation [*Becker and Tsoflias*, 2010].

Flow was induced using a variable speed positive displacement pump (Rediflo-2, Grundfos). Flow rates were minimized to maximize residence time of tracer in the formation. However, because there is strong natural flow in the fracture a minimum pumping rate (Q_R) needed to be maintained to get good tracer recovery. Pumping rates ranged between 1.0 and 4.1 L/min.

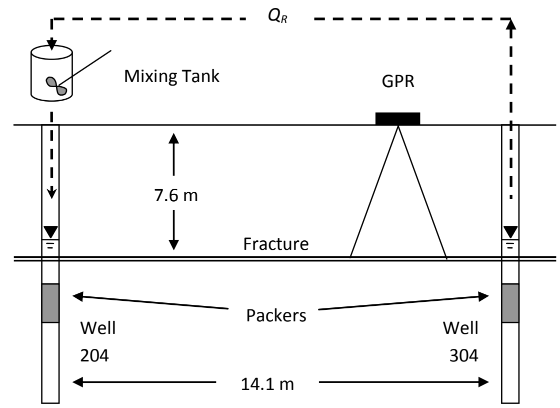

Figure 2: Schematic of the tracer test experimental set up. Tracer is circulated through a single bedding plane fracture via a well pair. The same fracture can be imaged using ground penetrating radar (GPR).

Tracer tests were initialized by creating a steady dipole flow field through pumping and re-injection (Figure 2). The test was initiated by adding a known mass of LiBr solution to the surface tank. The tracer mixed nearly instantly in the surface tank and then was gravity drained into the injection well. A packer in the injection well minimized the volume in the injection borehole to about 3 L which was also assumed to be fully mixed. This experimental design was chosen such that the flow field would be steady even while the tracer experiment was transient. Deconvolving the influence of transient flow fields and solute transport on breakthrough curves is, in our experience, nearly impossible.

Results of the tracer experiments are gathered in Figure 3. All breakthrough curves are plotted as Q_RC/Mo, where Q_R is the recirculation flow rate, Mo is the injected tracer mass and C is the measured concentration in the mixing tank. Because water was recirculated, the tracer was also recirculated and multiple peaks are visible in the breakthrough. The top two plots display the breakthrough between the corner wells 204-304 and 104-504, where 204 and 104 were the injection wells and 304 and 504 were the pumping wells. The remaining four plots display breakthrough in tracer experiments in which the center well, 404, was pumped and tracer was injected at the corner wells, 104, 204, 504, and 304.

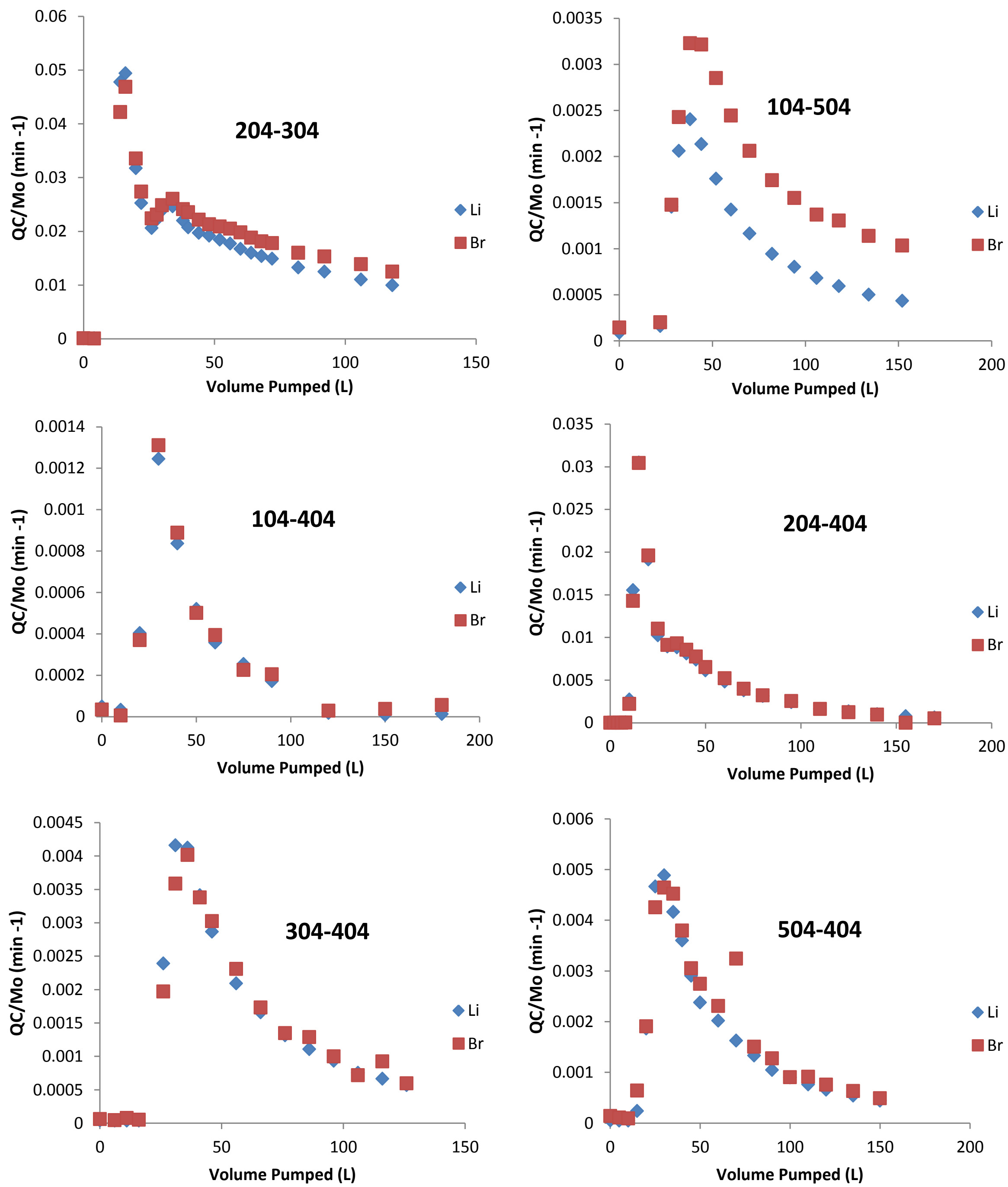

Figure 3: Breakthrough curves for lithium and bromide tracers. Well pairs are labeled as injection-pumping.

Mass recovery for the experiments varied widely. Because the traced water was recirculated, calculation of mass recovery by integration under the breakthrough curves (Figure 3) can result in greater than 100% mass recovery. Actual mass recovery was generally much less than 100%, however.

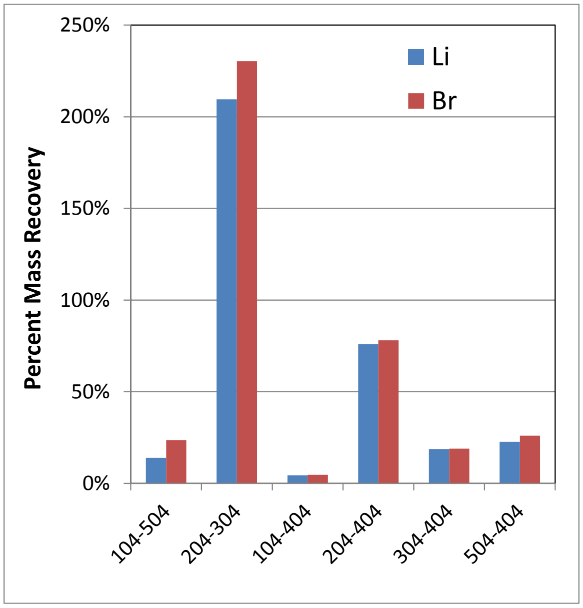

Figure 4: Percentage of injected tracer mass recovered during the tests (integration under the breakthrough curves of Fig. 3). Mass recovery can exceed 100% due to recirculation of traced water.

TRACER SIMULATION

The semi-analytical model RELAP (*Reimus et al.*, 2003) and numerical model MULTRAN (*Sullivan et al.*, 2003) were used in combination to interpret the separation in breakthrough between the anionic and cationic tracers, with a goal of estimating relative surface area to volume ratios in the active fractures in the 104-504 and 204-304 tests. The approach to interpreting the tracer breakthrough curves was to first use RELAP to fit the conservative bromide tracer responses, taking advantage of the extremely rapid computation times of the semi-analytical model to perform numerous trials to estimate transport parameters. A dual-porosity system was assumed, with a matrix porosity of 0.02 and a bromide matrix diffusion coefficient of 1 x 10^{-6} cm^2/sec.

The parameters estimated from RELAP were input to MULTRAN to simultaneously simulate/fit both the bromide and lithium breakthrough curves, adjusting only the average fracture aperture, or twice the fracture volume to surface area ratio (assuming parallel-plate fractures), to obtain a reasonable match to both data sets for each test. Because lithium and bromide were co-injected, the RELAP-estimated bromide transport parameters were also assumed to apply to lithium. Some iteration between MULTRAN and RELAP was allowed because fracture aperture estimates are better constrained by the simultaneous matching of the bromide and lithium breakthrough curves. Lithium cation exchange parameters are not well constrained for the Altona system, so published equilibrium constants for cation exchange reactions were used (*Appelo*, 1996), and a modest cation exchange capacity of 0.2 eq/kg was assumed for the matrix in both tests. Model trials indicate that the simultaneous first arrivals of the bromide and lithium are due to lithium-cation exchange in the matrix or in a weathered skin on fracture surfaces. As a consequence, all cation exchange reactions in the model were assumed to occur only in the matrix.

Figure 5 shows the MULTRAN fits to the test 204-304 breakthrough curves, with the estimated model parameters listed in Table 1. A fracture aperture estimate of 1 mm is approximately the smallest aperture that still provided a reasonable match to both tracer data sets given the assumed matrix diffusion and cation exchange parameters. Smaller apertures resulted in greater separation of the lithium and bromide curves than was experimentally observed.

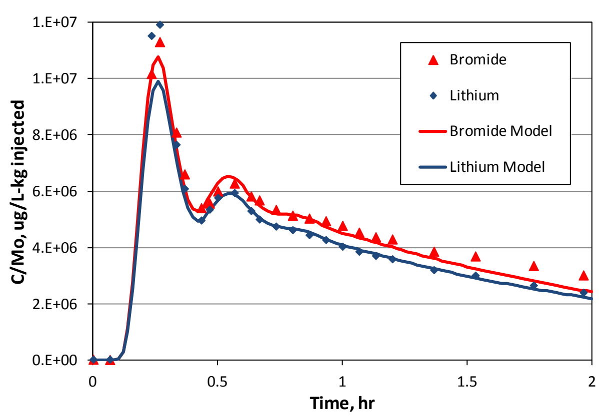

Figure 5: MULTRAN fits to the tracer breakthrough curves of test 204-304.

Matching the breakthrough curves from test 104-504 was more challenging. When a single fracture flow pathway was employed (as in the case of the 204-304 test), it was not possible to match both the early lithium peak and the significant separation between the tails of the lithium and bromide breakthrough curves. These features could be matched only by assuming that two separate flow pathways contributed to the tracer breakthrough curves; a faster pathway with larger fracture apertures that resulted in

Table 1. Estimated model parameters associated with fits of Figures 5 and 6.

Parameter	204-304	104-504 Pathway 1	104-504 Pathway 2
Tracer Mass Fraction	0.55	0.06	0.1
Mean Residence Time, hrs	0.27	0.65	1.1
Peclet Number	21	35	16
Fracture Aperture, mm	1.0	1.0	0.2

the early lithium peak, and a slower pathway with smaller apertures that explains the separation in the tails of the breakthrough curves.

Figure 6 shows both the single-pathway and the dual-pathway MULTRAN fits to the test 104-504 breakthrough curves. The wavy shapes of the dual-pathway model curves are an artifact of the empirical manner in which tracer recirculation was accounted for; recirculated tracer would normally be distributed between the two pathways in accordance with the flow distribution between pathways, but because RELAP and MULTRAN only simulate one pathway at a time, the distribution of recirculated tracer mass between the pathways could only be approximated. Despite the shortcomings of this approximation, the dual-pathway fit to the lithium breakthrough curve offers a substantial improvement over the single-pathway fit (with the bromide fit being compromised somewhat). The model parameters for the dual-pathway fit are listed in Table 1. It should be emphasized that the fits to the tracer curves were only semi-quantitative; no attempt was made to do a rigorous optimization of the fits because of the uncertainties in the underlying matrix diffusion and cation exchange parameters.

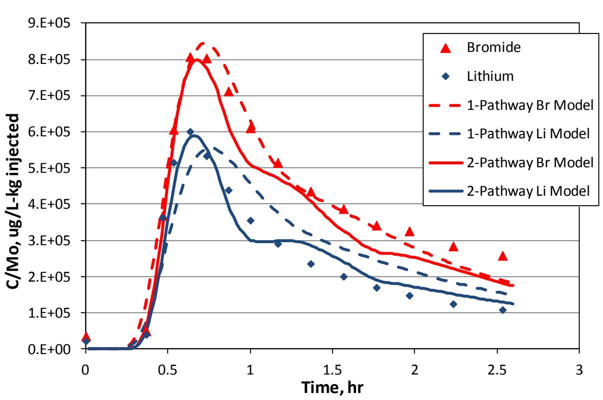

Figure 6: MULTRAN fits to the tracer breakthrough curves of test 104-504.

GROUND PENETRATING RADAR

Surface-based reflection GPR has been used at the field site to image saline tracer in multiple experiments [*Becker and Tsoflias*, 2010; *Tsoflias and Becker*, 2008]. In these experiments, saline water was introduced passively or injected under forced gradient while GPR was used to image its distribution and transport. In the imaging mode of interest here, saline water is circulated between well pairs while radar antennae are moved about the surface (Figure 5). Because reflection amplitudes were found to be affected by GPR signal polarization, antennae were oriented in parallel and orthogonally to the acquisition line and the amplitudes from both polarizations were summed [*Tsoflias et al.*, 2011]. The grid of these measurements, with spacing of 0.25m by 0.5m intervals, was contoured to produce “maps” of saline tracer migrating through the target fracture (Figure 6).

Figure 5: Photograph of GPR images being collected using the custom constructed multi-polarization antenna frame .

The change in electrical conductivity of water in the fracture results in a change in both amplitude and phase of the reflected GPR signal which may be used to estimate the relative mass of dissolved salt at the reflection horizon. The reader is referred to previous works regarding the theoretical and practical considerations of GPR imaging of saline fluid [*Tsoflias and Becker*, 2008]. It suffices here to note that the reflection amplitude is a function of both fracture aperture and saline concentration, and neither relationship is linear. However, if amplitude increase between pre-injection post-injection is mapped, the resulting variation in amplitude should be a function of saline concentration only.

Maps of reflected 100 MHz GPR amplitude difference (post-injection minus pre-injection) are displayed in Figure 6. The color scale represents reflected amplitude where more negative amplitudes represent the presence of saline tracer. The open circle represents the injection well and the filled circle the pumping well in each experiment. Asterisks denote wells used for monitoring. Due to difference between the pre- and post-tracer amplitudes, there is a significant amount of noise in the mapped reflections. However, it is apparent that the saline tracer is more widely dispersed in the test conducted between 104 and 504 than 204 and 304.

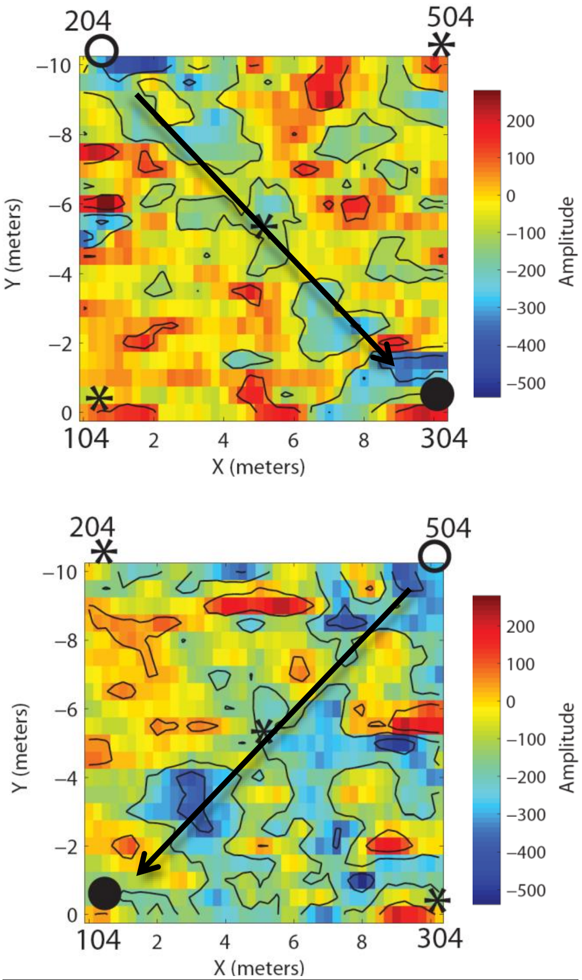

Figure 6: Saline tracer imaged by GPR. Blue color represents the presence of saline fluid circulated between wells 204 and 304 (top) or well 504 and 104 (bottom) (after Tsoflias et al., 2012).

DISCUSSION AND CONCLUSIONS

Trends in the tracer breakthrough curves (Figure 3) and mass recovery (Figure 4) are evident. First, mass recovery was highly dependent on the orientation of the test to the prevailing natural flow field. Based upon GPR imaging of passive tracer flow through the well field, the flow field appears to trend locally from west to east. This natural flow is generally in line with the head gradient (Figure 1) but is likely influenced by hydraulic anisotropy of the fractured formation. The experiment in which tracer was injected in 204 and recovered from 304 (in an eastward direction) saw 230% and 209% recovery of conservative bromide and reactive lithium tracers, respectively. The test in the perpendicular direction, 104-504, only saw 24% and 14% recovery of bromide and lithium, respectively.

However, tracer recovery is also affected by the hydraulic connection between well pairs. Well 104 is known to be less hydraulically connected to the target fracture than the other wells [*Becker and Guiltinan*, 2009]. Examining the tracer tests which were conducted from the corner wells to the central well; well 204 had the greatest conservation of tracer and 104 the poorest. Wells 304 and 504 also showed poor recovery, but this is likely because they are oriented perpendicular to the natural flow field.

The separation of cationic/anionic tracer break-through is negligible in all corner-well to center-well experiments (104-404, 204-404, 304-404, 504-404). Apparently, the inter-well distance of 7 m, and consequently the reactive surface area, is too small to result in differential sorption between ionic tracers. The separation of cationic/anionic tracer break-through is significant in corner-well to center-well experiments (104-504, 204-304). The greater inter-well distance of 14 m provided enough reactive surface area for the Li and Br tracers to behave differently during transport and to allow estimation of fracture surface areas interrogated by the tracers.

The fracture surface area to volume ratio estimate for the 204-304 test is simply the reciprocal of the estimated fracture half-aperture, which is 20 cm^2/cm^3, or 2000 m^2/m^3. For the 104-504 test, it is the volume-weighted average of the reciprocal half-apertures in the two-flow pathways. The volume in each flow pathway can be approximated by the product of the tracer mass fraction in the pathway, the tracer mean residence time, and the volumetric flow rate of pumping. Using values from Table 1, we estimate volumes of 9.36 L for the faster pathway and 26.4 L for the slower pathway.

The volume-weighted average of the reciprocal half-apertures is then 79.1 cm^2/cm^3, or 7910 m^2/m^3. We emphasize that the absolute estimates of fracture apertures are dependent on the assumed values of the matrix porosity, tracer matrix diffusion coefficients, and lithium cation exchange parameters, which are not well known at Altona. Even so, the model estimated apertures of 0.25 to 1.0 mm compare well with the 0.5 mm hydraulic aperture estimated from hydraulic tests. Although uncertainty in the absolute values of the a mean transport aperture is large, by assuming that the same parameters (other than apertures) apply to both tests, it is possible to obtain good estimates of *relative* apertures in the two tests. Thus, the surface area to volume ratio in the 104-504 test is estimated to be about 4 times greater than in the 204-304 test.

The overall fracture surface areas in each test can be estimated from the product of the surface area to volume ratio and the tracer-based volume in each test. For the 204-304 test, the tracer volume is estimated to be 36.9 L, and for the 104-504 test it is 9.36 + 26.4 = 35.8 L (i.e., nearly the same total volume in each test, with the lower tracer recoveries in the 104-504 test being offset by the longer tracer residence times in this test). Using the surface area to volume ratios provided above, it is estimated that the overall surface area in the 104-504 test is about 3.8 times greater than in the 204-304 test.

Given that the overall fracture surface area should approximately translate to a 2-D (plan-view) area in the Altona single-fracture system, the relative surface area estimates for the two well pairs are qualitatively consistent with the imaging of saline tracer among the well pairs (Figure 6). Quantitatively, the surface relative surface areas of saline fluid estimated by the GPR imaging appears to be only about 1.5 times as large in the 104-504 test than the 204-304 test. This estimate, however, is based on simple image interpretation of the threshold concentrations displayed in Figure 6. Saline concentration was not accounted for. Processing of the GPR data continues and will produce a more quantitative measure of the ratio of surface volume to area.

In general, the tracer results confirm the conceptual model of flow in the fracture. Saline tracer is conducted in a relatively direct path between 204 and 304 because the flow path aligns with the natural flow direction and because these wells are strongly hydraulically connected. Previous imaging and hydraulic tests suggest that the hydraulic conductivity field is strongly anisotropic, favoring flow in this east-west direction [*Becker and Tsoflias*, 2010; *Tsoflias et al.*, 2011]. The saline tracer and, presumably, the ionic tracers, follow an induced flow channel that connects the wells.

In the well pair, 104-504, the flow field is much more disperse. Such a disperse flow field is expected when flow is induced orthogonal to a strong anisotropic hydraulic conductivity field. Thus, the poor hydraulic connection actually leads to a better sweep of the formation than the good hydraulic connection. As fracture networks tend to promote flow channeling, one might conjecture that it will be increasing difficult to maintain a good sweep of the formation at larger scales. The reader should be cautioned, however, that his simple relationship is complicated in these experiments by the presence of a strong natural flow field parallel to the principal direction of the hydraulic conductivity tensor. We are in the process of performing two-dimensional flow modeling that accounts for the natural gradient to achieve a more robust interpretation of these tracer experiments.

REFERENCES

Andersson, P., et al. (2002), Final report of the TRUE Block Scale Project: 2. Tracer tests in the block scale, SKB-TR-02-14, Swedish Nuclear Fuel and Water Management Co. (SKB), Stockholm, Sweden.

Appelo C.A.J. (1996), Multicomponent ion exchange and chromatography in natural systems. In: *Reactive Transport in Porous Media*. PC Lichtner, CI Steefel, and EH Oelkers (Editors). *Reviews in Mineralology* 34:193–227.

Becker, M. W., and A. M. Shapiro (2003), Interpreting tracer breakthrough tailing from different forced-gradient tracer experiment configurations in fractured bedrock, *Water Resources Research*, *39*(1).

Becker, M. W., and E. Guiltinan (2009), Cross-hole periodic hydraulic testing of inter-well connectivity, in *Thirty-Fifth Workshop on Geothermal Reservoir Engineering*, edited, Stanford University, Stanford, California.

Becker, M. W., and G. P. Tsoflias (2010), Comparing Flux-Averaged and Resident Concentration in a Fractured Bedrock using GPR, *Wat. Resour. Res.*, *46*, W09518, doi: 09510.01029/02009WR008260.

Callahan, T. J., et al. (2000), Using multiple experimental methods to determine fracture/matrix interactions and dispersion of nonreactive solutes in saturated volcanic tuff, *Water Resources Research*, *36*(12), 3547-3558.

Castagna, M., et al. (2011), Joint estimation of transmissivity and storativity in a bedrock fracture, *Water Resources Research*, *47*.

Dean, C., et al. (2012), Evaluation of a cation exchanging tracer to interrogate fracture surface area in EGS systems, paper presented at Thirty-Seventh Workshop on Geothermal Reservoir Engineering, Stanford

University, Stanford, California, January 30 - February 1, 2012, SGP-TR-194.

Guiltinan, E. J., and M. Becker (2010), Using harmonic hydraulic tests to estimate fractured bedrock properties and predict local heterogeneity, *Abstracts with Programs - Geological Society of America*, *42*(4), 110.

Hawkins, A. J., and M. W. Becker (2012), Measurement of the spatial distribution of heat exchange in a geothermal analog bedrock site using fiber optic distributed temperature sensing, paper presented at Thirty-Seventh Workshop on Geothermal Reservoir Engineering Stanford University, Stanford, California, January 30 - February 1, 2012 SGP-TR-194.

Rayburn, J. A., et al. (2005), A series of large, Late Wisconsinan meltwater floods through the Champlain and Hudson Valleys, New York State, USA, *Quaternary Science Reviews*, *24*(22), 2410-2419.

Reimus, P. W., et al. (2003), Testing and Parameterizing a Conceptual Model for Radionuclide Transport in a Fractured Granite using Multiple Tracers in a Forced-Gradient Test, *Water Resources Research*, 39(12), 1350, doi:10.1029/2002WR001597.

Reimus, P. W., and T. J. Callahan (2007), Matrix diffusion rates in fractured volcanic rocks at the Nevada Test Site: Evidence for a dominant influence of effective fracture apertures, *Water Resources Research*, *43*(7).

Shook, G. M., and J. H. Forsmann (2005), Tracer interpretation using temporal moments on a spreadsheet, INL/EXT-05-00400, Idaho Falls, Idaho.

Sullivan, E. J., et al. (2003), "Transport of a reactive tracer in saturated alluvium described using a three-component cation-exchange model," *J. Contaminant Hydrology*, v. 62/63, p. 675-694.

Talley, J., et al. (2005), Four dimensional mapping of tracer channelization in subhorizontal bedrock fractures using surface ground penetrating radar, *Geophys. Res. Lett.*, *32* (doi:10.1029/2004GL021974).

Tester, J., and others (2006), The Future of Geothermal Energy, Impact of Enhanced Geothermal Systems (EGS) on the United States in the 21st Century: An Assessment Massachusetts Institute of Technology, Cambridge, Massachusetts.

Tsoflias, G. P., and M. W. Becker (2008), Ground-penetrating-radar response to fracture-fluid salinity: Why lower frequencies are favorable for resolving salinity changes, *Geophysics*, *73*(5), J25-J30.

Tsoflias, G. P., et al. (2011), Abstract NS41A-07, Assessing GPR Signal Polarization for 3D Imaging of Fracture Flow Channels presented at 2011 Fall Meeting, AGU, San Francisco, Calif., 5-9 Dec.

Appendix D

Hawkins, A. J., and M. W. Becker (2012), Measurement of the spatial distribution of heat exchange in a geothermal analog bedrock site using fiber optic distributed temperature sensing, paper presented at *Thirty-Seventh Workshop on Geothermal Reservoir Engineering,* Stanford University, Stanford, California, January 30 - February 1, 2012 SGP-TR-194.

PROCEEDINGS, Thirty-Seventh Workshop on Geothermal Reservoir Engineering
Stanford University, Stanford, California, January 30 - February 1, 2012
SGP-TR-194

MEASUREMENT OF THE SPATIAL DISTRIBUTION OF HEAT EXCHANGE IN A GEOTHERMAL ANALOG BEDROCK SITE USING FIBER OPTIC DISTRIBUTED TEMPERATURE SENSING

Adam J. Hawkins and Matthew W. Becker

California State University, Long Beach, Geology Department
1250 Bellflower Boulevard
Long Beach, California, 90840, USA
ajjhawkins@gmail.com matt.becker@csulb.edu

ABSTRACT

Highly channelized flow in fractured geologic systems has been credited with early thermal breakthrough and poor performance of geothermal circulation systems. An experiment is presented here in which the effect of channelized flow on fluid/rock heat transfer is measured. Hot water was circulated between two wells in a single bedding plane fracture and the elevation of rock matrix temperature was measured using fiber optic Distributed Temperature Sensing (DTS). Between wells with good hydraulic connection, heat transfer appeared to follow a classic dipole sweep pattern. Between wells with poor hydraulic connection, heat transfer was skewed toward apparent regions of higher transmissivity (or larger aperture). These results are consistent with hydraulic and tracer tests, as well as ground penetrating radar imaging, that shows a heterogeneous distribution of transmissivity. Although these results are preliminary and still qualitative, they suggest that flow channeling can have a significant impact on heat transfer efficiency even in single planar fractures.

INTRODUCTION

Enhanced Geothermal Systems (EGS) are heavily dependent on creating a sufficient surface area through which heat may be exchanged between flowing fluid in fractures and the surrounding hot rock matrix. In geothermal reservoirs characterized by tight interconnected fractures, water flows unevenly in response to injection and pumping. Uneven flow or flow “channeling” can lead to premature thermal breakthrough and, therefore, is a critical design parameter for effective EGS.

Tracer testing has become a standard tool for the prediction of early breakthrough. Over 100 tests have been conducted in geothermal reservoirs [*Shook and Forsmann*, 2005]. The vast majority of these tests have utilized conservative (non-reactive) tracers to measure residence time among well pairs. Recent advancements have produced "smart" tracers which can provide more detailed characterization of fractures, including surface area [*Tester and others*, 2006]. While theoretically viable and numerically validated, tracer tests have not been compared to independent measurements of effective surface area in field experiments. Here, an experiment is conducted in which heat exchange between circulated water in fractures and the bulk rock matrix is measured independently from the water temperature. These tests will be used to validate tracer measurements that will be presented elsewhere.

EXPERIMENTAL METHOD

The field site is located in Altona Flat Rocks, in northern New York, USA about 4 miles northwest of West Chazy, New York. Altona Flat Rocks is highly unique in the Northeastern United States, because a glacial flood stripped soil overburden off of bedrock, exposing an expanse of sandstone with shallow groundwater in bedrock fractures [*Rayburn et al.*, 2005]. The natural flow of groundwater is to the Southeast and occurs only in fractures due to the low porosity of the well cemented Cambrian-aged Potsdam Sandstone formation. The proximity of the water table to the bare rock surface permitted imaging of fracture planes and saline tracer migration with ground penetrating radar (GPR) [*Becker and Tsoflias*, 2010; *Talley et al.*, 2005; *Tsoflias and Becker*, 2008]. A five-spot 15 cm diameter well pattern penetrates a conductive sub-horizontal fracture 7.6 m meters below the surface. For this project, an additional ten 15 cm diameter boreholes were drilled to a depth 60 cm above the conductive fracture for temperature monitoring of the dry rock matrix.

Temperature in the rock matrix above the fracture was measured using a fiber optic Raman scattering Distributed Temperature Sensing (DTS) system. Raman DTS measures temperature by measuring photon backscatter from laser transmission along a standard fiber optic cable. The ratio of Stokes and Anti-Stokes backscatter wavelengths is used to measure temperature while time of flight is used to position the temperature along the cable [*Tyler et al.*, 2009]. The system used at Flat Rock is a Sensornet Oryx, which records temperature every 1 m along the cable with a stated accuracy of 0.02 C when backscatter is integrated over a period of 10 minutes as in our experiments.

Because the native spatial resolution of 1 m along the fiber optic cable, the cable was wrapped around a threaded 5.71 cm outer diameter schedule-80 PVC pipe to increase the spatial resolution to 2.1 cm. Our laboratory tests indicate the instrument is not capable of distinguishing between strong temperature contrasts less than 5 cm apart, however. A special high numerical aperture cable was used for this purpose to reduce attenuation of signal due to the fiber curvature. Wrapping was facilitated using a standard machine tool lathe fitted with a retaining adapter (Figure 1). During the winding process, the fiber was wrapped with electrical tape to hold the fiber in place and protect it during installation (Figure 2). Five 3-meter long sensors and five 1.5-meter long sensors were created and tested on the campus of CSU Long Beach then shipped to the Flat Rock field site.

Figure 1: Process of wrapping fiber optic cable around a threaded PVC pipe assisted by a lathe.

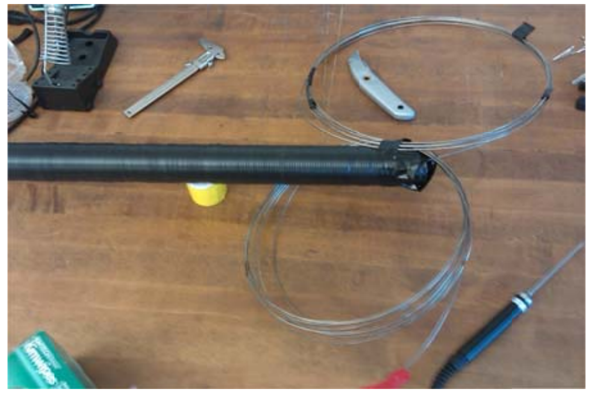

Figure 2: Close up of threaded PVC pipe wrapped with fiber optic cable and secured with electrical tape.

During July, 2011, all ten Sensor rods were installed into each of the ten boreholes. The ends of each sensor rod were fused to an adjacent borehole's sensor rod, creating a network that could be used to measure temperature along one continuous cable. The 8.26 cm annulus created between the sensor rods and the borehole wall was filled with a mixture of sand and water to create thermal coupling with similar thermal conductivity as the low porosity sandstone. A 3 cm horizontal layer of clay was added every 76 cm during backfilling to diminish the potential for pore water convection in the annulus. Unfortunately, two of the sensors were damaged by vandals during the team's absence from the field and could not be repaired in time for the experiments.

The thermal experiments were conducted by circulating heated water between the center and a corner well in the five spot (Figure 3). Two circulation experiments were conducted: (1) injection in 404 and pumping from 304 and (2) injection in 404 and pumping from 104. These wells were chosen because they were adequately covered by the partially crippled temperature sensor network. Fortunately, these wells allowed us to compare circulation with wells that were well-connected (304) and poorly-connected (104) hydraulically

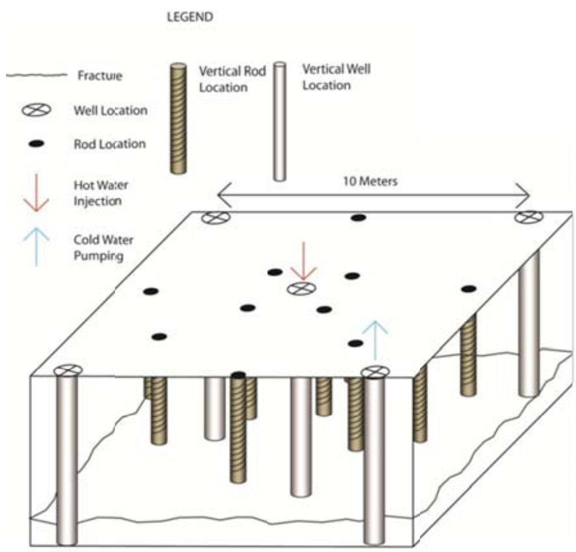

Figure 3: A schematic of the thermal experiments conducted in fractured bedrock.

Water for the experiments was heated using a propane-fired spa heater that maintained a constant 40ºC temperature in an 800 L source tank (Figure 4). This water temperature was approximately 30ºC warmer than temperature of the sandstone prior to the experiment. Water was circulated by gravity drainage into well 404 and return pumping from well 304 or 104 using a Grundfos MP1 adjustable speed pump. All wells were hydraulically isolated to the target fracture using inflatable straddle packers that limited fluid movement within 15 cm above or below the fracture. Temperature and head were monitored using self-contained loggers (Solnst, Waterloo, Ontario) in all wells within the straddled intervals.

Figure 4: A photograph of the experimental site. The DTS instrument, spa-heater, and storage tank are visible near well 404.

The two (404-304, 404-104) thermal experiments were conducted from October 4th to October 8th, 2011. The circulation between well 404 and 304 ran with an injection/pumping rate of 4 liters per minute for 46.5 hours and then the rate was increased to 8 liters per minute for an additional 7 hours to reduce the duration of the experiment. Circulation between well 404 and 104 ran with an injection/pumping rate of 8 liters per minute for 22.2 hours. During the 404-304 experiment, temperature in the pumped water raised 4 ºC and in the 404-104 experiment, only 1 ºC.

PRELIMINARY RESULTS

Because experiments were completed in October, 2011, at this writing only preliminary interpretations are available. It is clear, however, that heat exchange between the warm circulated water and the rock matrix was measured by the DTS sensor system. DTS measurements show heat propagating vertically above the fracture for both the 404-304 experiment (Figure 5) and 404-104 experiment (Figure 6). The maximum temperature rise in the rock matrix was approximately 6ºC during the 404-304 experiment and approximately 3ºC during the 404-104 experiment.

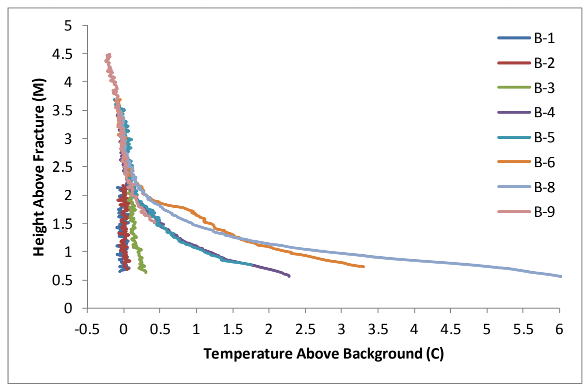

Figure 5: Temperature increase above background measured in the rock matrix during the 404-304 test using the DTS sensor.

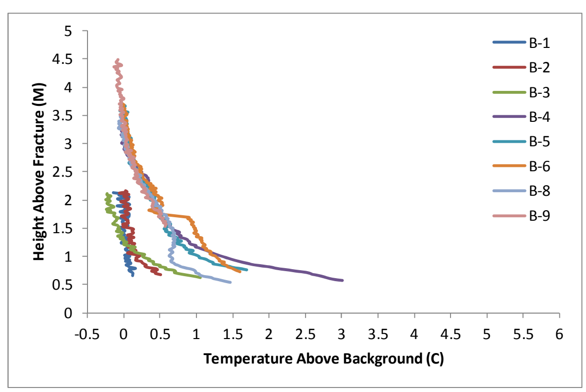

Figure 6: Temperature increase above background measured in the rock matrix during the 404-104 test using the DTS sensor.

DISCUSSION

The temperature profiles show the expected shape due to diffusion of heat from a constant heat source. The profiles are not predicted exactly by such a simple theoretical model, however, because (1) the temperature of circulated water in the fracture was not constant in time or space and (2) at the initiation of the second test the rock matrix temperatures had not returned entirely to background temperature. Analytical modeling is underway to assess the rate of heat transfer between the fracture and matrix. In the meantime, we offer a qualitative presentation of the heat exchange observed during the experiments.

Warm water circulation between well 404 and 304 elevated the rock matrix temperature in a manner consistent with a "dipole" circulation flow pattern. The greatest increase was measured just upstream (B-8) and just downstream (B-6) of well 404 (Figure 7). A lesser increase was observed in the next nearest lateral boreholes (B-4 and B-9). Wells intercepted by the longest theoretical dipole flow paths, (B-1, B-2, B-3) showed little or no increase in temperature.

The circulation between well 404 and 104 elevated the rock matrix temperature in a manner inconsistent with a "dipole" circulation flow pattern. This experiment showed an asymmetric distribution of temperature about the imaginary line connecting wells 404 and 104. The greatest temperature increase was again measured just downstream (B-4) of well 404, but the next well in direct path to 104 showed little temperature change. Both the proximate lateral wells, B-8 and B-6 showed an increase in temperature but the more distal wells to the East (B-3, B-5) also showed an increase. The propagation of the thermal front, therefore, appears to be skewed eastward in the 404-104 experiment.

The asymmetric distribution of heat about the circulating wells 404 and 104 is consistent with other studies from the site. Pump testing shows a relatively poor hydraulic connection between well 104 and the remaining wells [*Castagna et al.*, 2011]. GPR imaging of saline tracer suggested more efficient transport between wells 204-304 than wells 504-104 [*Talley et al.*, 2005]. A GPR measured tracer experiment, in which saline water was circulated between well 204 and 304 and imaged with stationary antennae place between 404 and 304, showed strong breakthrough consistent with a direct flowpath [*Becker and Tsoflias*, 2010]. Finally, recent GPR imaging of the target fracture without saline tracer suggests that apertures are generally larger in the region between wells 404 and 304 than they are between 404 and 104 [*Tsoflias et al.*, 2011].

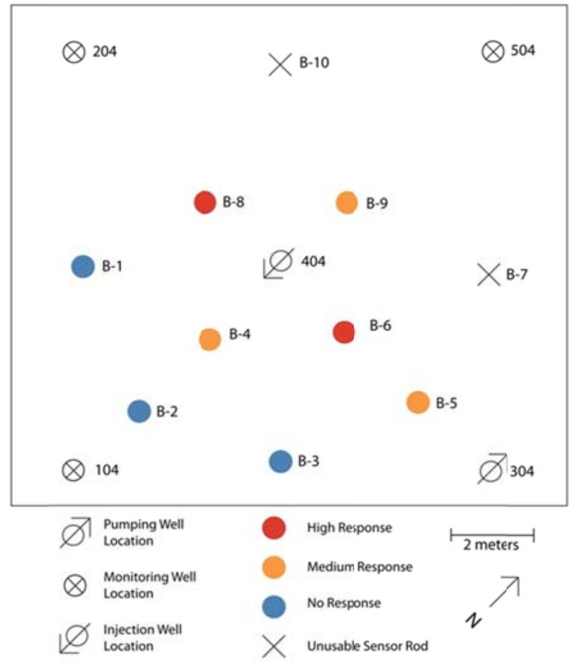

Figure 7: Classification of temperature response realized in the rock matrix during the 404-304 circulation experiment.

Figure 8: Classification of temperature response realized in the rock matrix during the 404-104 circulation experiment.

CONCLUSIONS

The heat transfer experiment produced useful results in spite of the loss of some equipment due to vandalism. Elevated temperatures in the sandstone matrix were measured in response to hot water circulated through the single bedding plane fracture. Heat transfer from the fracture to the rock matrix was highly symmetrical between two wells situated in a well-connected region of the study fracture, suggesting a classic dipole water sweep. Heat transfer was less symmetrical between two wells known to have poorer hydraulic connection. In this experiment, heat transfer appears to have been diverted to a more conductive region of the study area due to flow channeling. The experiment appears to lend support to the impact of channelized flow, even in single planar fractures. These results are only preliminary and qualitative, however. Modeling is underway to better constrain the results and interpretation.

REFERENCES

Becker, M. W., and G. P. Tsoflias (2010), Comparing Flux-Averaged and Resident Concentration in a Fractured Bedrock using GPR, *Wat. Resour. Res.*, **46**, W09518, doi: 09510.01029/02009WR008260.

Castagna, M., et al. (2011), Joint estimation of transmissivity and storativity in a bedrock fracture, *Water Resources Research*, **47**.

Rayburn, J. A., et al. (2005), A series of large, Late Wisconsinan meltwater floods through the Champlain and Hudson Valleys, New York State, USA, *Quaternary Science Reviews*, **24**(22), 2410-2419.

Shook, G. M., and J. H. Forsmann (2005), Tracer interpretation using temporal moments on a spreadsheet, INL/EXT-05-00400, Idaho Falls, Idaho.

Talley, J., et al. (2005), Four dimensional mapping of tracer channelization in subhorizontal bedrock fractures using surface ground penetrating radar, *Geophys. Res. Lett.*, **32** (doi:10.1029/2004GL021974).

Tester, J., and others (2006), The Future of Geothermal Energy, Impact of Enhanced Geothermal Systems (EGS) on the United States in the 21st Century: An Assessment Massachusetts Institute of Technology, Cambridge, Massachusetts.

Tsoflias, G. P., and M. W. Becker (2008), Ground-penetrating-radar response to fracture-fluid salinity: Why lower frequencies are favorable for resolving salinity changes, *Geophysics*, **73**(5), J25-J30.

Tsoflias, G. P., et al. (2011), Abstract NS41A-07, Assessing GPR Signal Polarization for 3D Imaging of Fracture Flow Channels presented at 2011 Fall Meeting, AGU, San Francisco, Calif., 5-9 Dec.

Tyler, S. W., et al. (2009), Environmental temperature sensing using Raman spectra DTS fiber-optic methods, *Water Resources Research*, **45**.

Appendix E

Tsoflias, G. P., C. Perll, M. Baker, and M. W. Becker (2014), Investigation of cross-polarized GPR signals for imaging fracture flow channeling, in *6th International Conference on Environmental and Engineering Geophysics,* June 20-23, 2014, edited, Xi'an, China.

Investigation of cross-polarized GPR signals for imaging fracture flow channeling

Georgios Tsoflias[1], Christopher Perll[1,2], Matthew Baker[1] and Matthew Becker[3]
1. Department of Geology, The University of Kansas, Lawrence, KS, USA
2. Chesapeake Energy, Oklahoma City, OK, USA
3 California State University Long Beach, Long Beach, CA, USA

Abstract

Ground penetrating radar (GPR) can be used to image fractured rock and monitor the flow of fluids in the subsurface. Conventional GPR imaging uses single-polarization, co-polarized signals. This study investigates if cross-polarized GPR signals can image channeling at a discrete horizontal fracture. To assess the response of cross-polarized radar waves to fracture channels 3D FDTD numerical models were used to simulate varying fracture properties (i.e. aperture, channel orientation, fracture water electrical conductivity) and mulitpolarization GPR field data were acquired to monitor saline tracer tests in a subhorizontal fracture.

Numerical modeling demonstrated that the cross-polarized data are able to image fracture channels when the axis of the channel is oriented obliquely to the EM wavefield orientation. When the fracture channel is oriented at an oblique angle to the survey line, depolarization of the GPR signal results in scattered energy along the cross-polarized components. Summation of the cross-polarized and co-polarized components results in an accurate representation of the total scattered energy from the channel. When the channel is oriented parallel or orthogonal to the survey line all scattered energy is captured by the co-polarized components.

Multipolarization, time-lapse 3D GPR field data were acquired at the Altona Flat Rock test site in New York State to investigate GPR imaging of flow channeling in a discrete subhorizontal fracture. The GPR surveys were conducted during background fresh fracture water conditions and during a natural gradient saline tracer test which is used to highlight flow channels at the site. Amplitude analysis of the cross-polarized data reveals flow channeling which is in agreement with the co-polarized GPR data and with independent hydraulic tests. In conclusion, this investigation demonstrates for the first time that cross-polarized components of GPR signals can be used to enhance imaging of channels and monitoring of flow in fractured media.

Keywords: Ground penetrating radar, polarization, fracture, channel, fluid flow.

Introduction

Ground penetrating radar (GPR) has been used to image fractures and monitor contaminants (Davis and Annan, 1989; Tsoflias et al., 2001; Day-Lewis et al., 2003; Talley et al., 2005; Deparis and Garambois, 2009; Dorn et al., 2011, 2012). Commonly GPR investigations employ single-polarization co-polarized GPR data which are adequate for imaging planar subhorizontal interfaces. However, flow in fractured rock occurs along preferential pathways of varying aperture referred as flow channels (Tsang and Neretnieks, 1998). Depending on the polarization of the incident wave and the orientation of the target the radar wave can be preferentially scattered (Roberts and Daniels, 1996) which causes changes in the reflected signal amplitude. Acquiring multipolarization GPR data has been shown to provide more precise measurements of the size, shape, and orientation of the target (Roberts and Daniels, 1996; Lehmann et al., 2000; Radzevicius and Daniels, 2000; Sato and Miwa, 2000; Tsoflias et al., 2004). Tsoflias et al. (2012) observed significant differences in fracture reflection amplitude between orthogonally oriented parallel-polarized signals and showed that summation of the orthogonally oriented wavefields improved imaging of fracture channels. The work presented here examines if cross-polarized signals can improve GPR imaging of fracture channels. We employ FDTD numerical modeling and field data to investigate the GPR response of flow channeling along a subhorizontal fracture.

Numerical Modeling

Methods:

Three-dimensional FDTD modeling (GprMax V 2.0; Giannopoulos, 2005) was used to simulate 50 MHz and 100 MHz orthogonally oriented co-polarized (P1, P3) and cross-polarized (C1, C3) GPR profiles over a horizontal planar fracture containing a channel oriented perpendicular (0^o) and oblique (45^o) to the plane of incidence. The fracture channel was modeled by overlaying a cylinder to the fracture plane. The four polarizations simulated and the models with the perpendicular and oblique channel orientations are shown in figure 1.

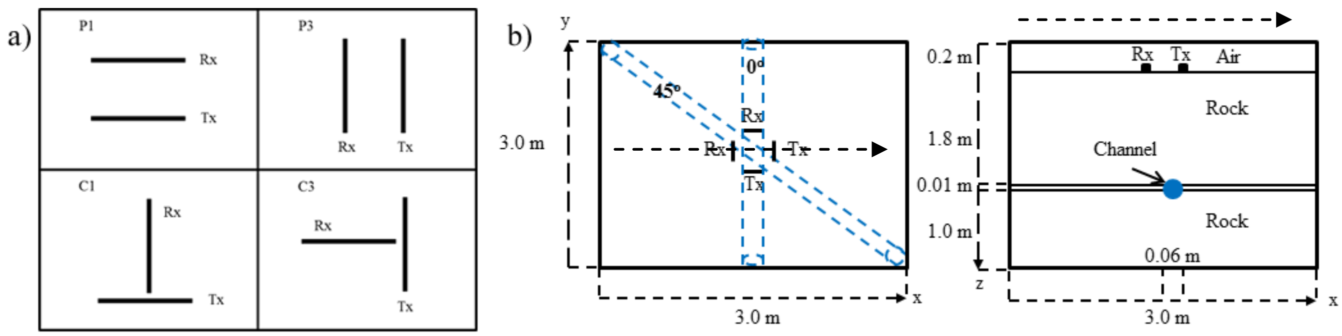

Figure 1: a) Co-polarized (P1, P3) and cross-polarized (C1, C3) source and receiver orientations (Tx: source; Rx: receiver). b) 3D FDTD model geometry. (left) Map view showing co-polarized source and receiver locations, 0^o and 45^o oriented channels. (right) Cross-section view of the model with a 0.01 m aperture fracture containing a 0.06 m diameter channel (model not to scale). Arrow indicates the simulated survey line orientation along the x-axis.

Model parameters were set to simulate the Altona Flat Rock field site: rock-matrix dielectric constant $\varepsilon_r = 7$, electrical conductivity $\sigma = 0$ mS/m, water $\varepsilon_r = 80$ and $\sigma = 28$ mS/m. Fracture aperture was set to 0.01 m, channel diameter 0.06 m and channel σ was increased to 180 mS/m, 400 mS/m, and 700 mS/m to simulate varying saline tracer concentration comparable to field hydraulic tracer tests. Individual radar traces were simulated with the fracture channel centered below the transmitting and receiving antennae and survey line profiles were run through the middle of the model along the x-axis.

Results:

Simulated 50 MHz unmigrated GPR lines over a horizontal planar fracture containing a cylindrical channel are shown in figure 2. Reflected signal in the co-polarized components P1 and P3 (Figure 2a) is dominated by the horizontal planar fracture interface which masks the presence of the cylindrical channel. Weak evidence of the channel may be inferred by diffracted energy in the P3, 0^o channel profile (Figure 2a, lower right panel). The sum of co-polarized components P1+P3 shown in figure 2b is also dominated by the planar fracture reflection and does not provide evidence of the presence of the channel. Figure 2c shows the difference between a model of the fracture including a channel and a model of the planar fracture without a channel. Figure 2c reveals the diffraction from the cylindrical channel contained in 2b. The cross-polarized components C1 and C3 and the sum C1+C3, image the channel when oriented at an oblique angle to the EM wavefields (Figures 2d and 2e left

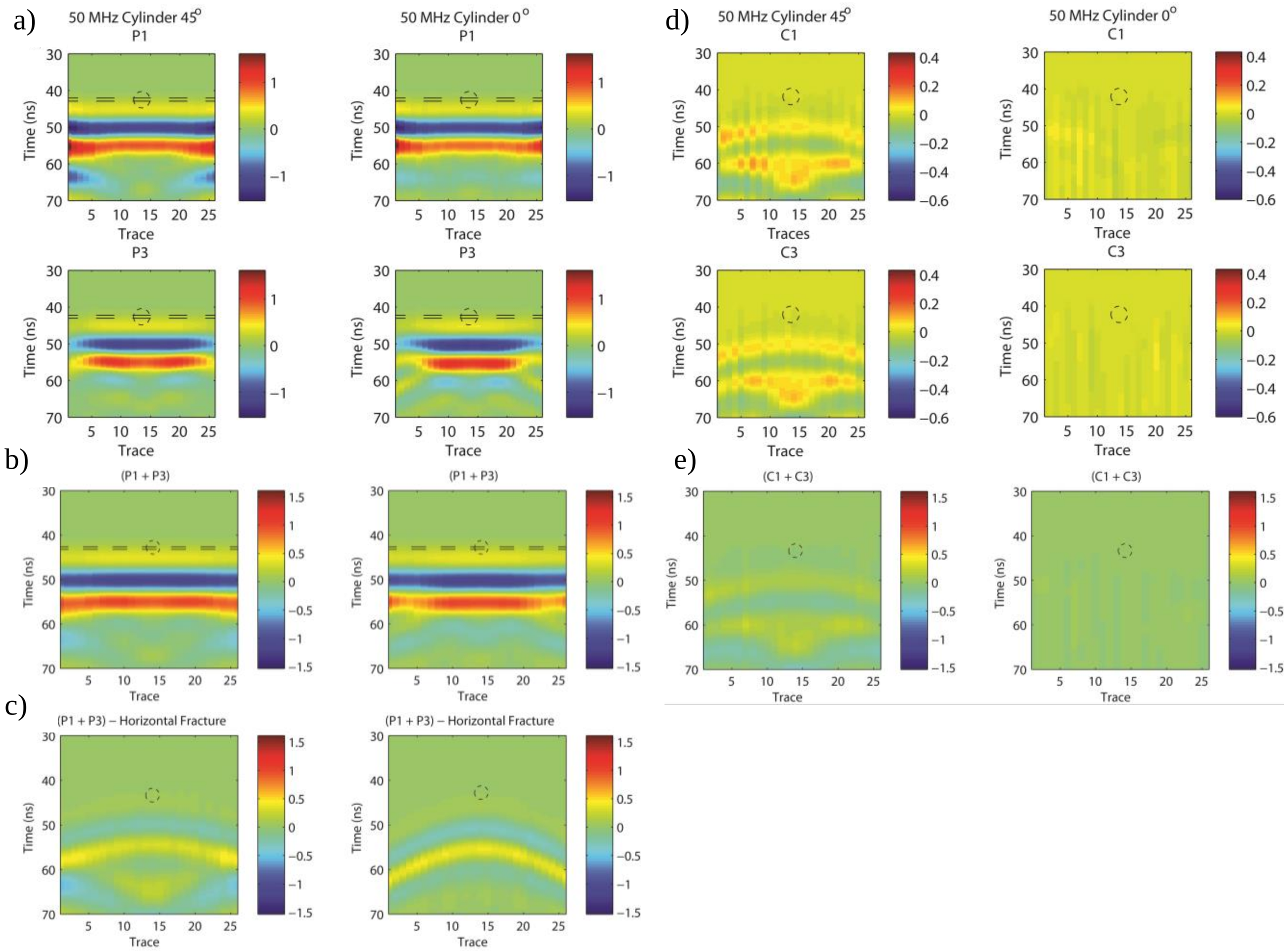

Figure 2: Unmigrated 50 MHz survey line over horizontal planar fracture with cylindrical channel. (Left) 45^0 channel and (Right) 0^0 channel. Water electrical conductivity of 28 mS/m. a) Co-polarized P1 and P3 wavefield components, b) Sum (P1+P3) of co-polarized components, c) Horizontal fracture model without channel subtracted from 2b (P1+P3), d) cross-polarized C1 and C3 components, e) Sum (C1+C3) of cross-polarized components.

panels). When the channel is oriented parallel and perpendicular (i.e. 0^o) to the receiving and transmitting antennae no appreciable reflected energy is oriented along the cross-polarized components (Figures 2d and 2e right panels). In addition, no cross-polarized component reflections result from the planar fracture interface.

Numerical modeling observations can be summarized as follows:

1. Co-polarized signals are dominated by the planar horizontal fracture reflection. The weak reflection from the narrow cylindrical channel (0.06 m in diameter compared to 2 m wavelength of the 50 MHz signal) is masked by the high amplitude fracture plane reflection.
2. Cross-polarized signals detect the channel when it is oriented at an oblique angle to the EM wavefields. Furthermore, the cross-polarized components do not detect the horizontal fracture.
3. Subtracting the horizontal fracture from the co-polarized components yields an image of the oblique channel that is similar to the cross-polarized image of the oblique channel. Comparison of the two images (Figure 2c left vs. 2e left) shows that the cross-polarized signals are lower in amplitude and reverse in polarity compared to the co-polarized signals.

Field Experiment

Methods:

Three-dimensional (3D) multipolarization time-lapse GPR data were collected at the Altona Flat Rock site located approximately 15 km northwest of Plattsburg, NY. The site is instrumented with five boreholes that are used to conduct tracer tests through a hydraulically conductive subhorizontal fracture 7.6 m below ground surface. The 3D GPR grids covered approximately a 100 m^2 area at 0.25 m x 0.5 m trace spacing (Figure 3a). Radar data were acquired at 50 MHz and 100 MHz frequencies using a multichannel GPR system with two transmitters and two receivers (Figure 3b). Co- and cross-polarized dipole antenna pairs were oriented parallel and orthogonal to the survey grid lines. Field GPR data consisted of simultaneous acquisition of P1, P3, C1 and C3 components at each survey location. In this study we present cross-polarized GPR imaging of a natural gradient hydraulic test. Saline tracer was injected upgradient in borehole 204 and was transported by the natural gradient to the east across the survey area. Time-lapse GPR data were collected at background conditions prior to the injection of the tracer and during the natural gradient tracer test.

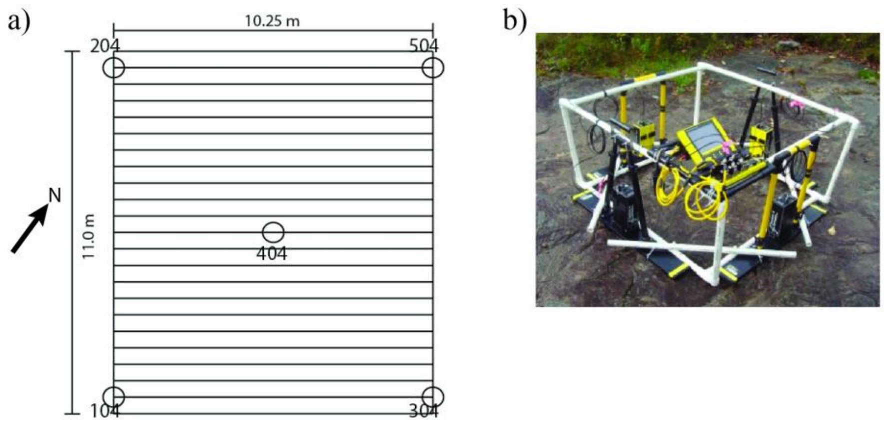

Figure 3: a) Schematic of field site showing borehole locations (open circles) and GPR grid lines. b) Multichannel GPR system shown with 100 MHz antennae.

Results:

Figure 4 shows 50 MHz amplitude maps of the 7.6 m fracture reflector for background (fresh) water salinity (Figures 4a and c) and saline fracture water during the natural gradient test (Figures 4b and d). Amplitude maps are shown for the summed cross-polarized (C1+C3) (Figures 4a and b) and co-polarized (P1+P3) components (Figures 4c and d). Large negative GPR amplitudes of the co-polarized fresh water fracture background data (Figure 4c) suggest a greater fracture aperture region (channel) oriented East-West, from well 204 to 304. Increasing fracture water salinity is expected to result in increased fracture reflection amplitude (Talley et al., 2005; Tsoflias and Becker, 2008). The co-polarized natural gradient tracer test GPR amplitude data (Figure 4d) further highlight the East-West channel along the fracture plane. The cross-polarized background data (Figure 4a) shows overall weak amplitudes with no well-defined spatial trend. Low amplitude variability of the cross-polarized signal is likely the result of fracture surface roughness (Sato and Miwa, 2000). Increased water salinity during the natural gradient tracer test results in significant increase of the cross-polarized signal amplitudes (Figure 4b). The cross-polarized amplitudes trend in an East-West orientation, which is oblique to the NE-SW orientation of the survey lines. The fracture channels revealed by the cross-polarized amplitudes during the natural gradient test are in good agreement with the co-polarized amplitude data. Therefore, the cross-polarized radar data is able to detect in the field fracture flow channels which are oriented oblique to the GPR survey lines.

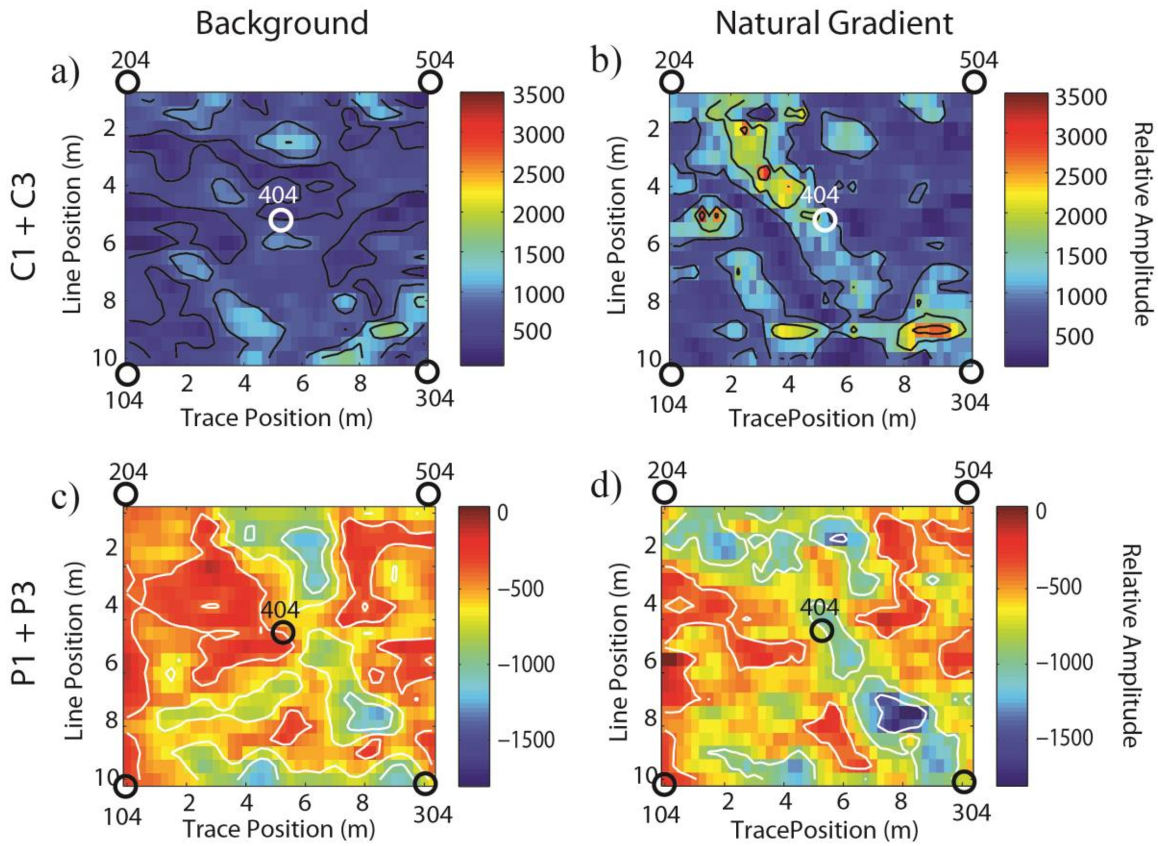

Figure 4: Fifty MHz amplitude maps of the 7.6 m fracture reflector a) Cross-polarized sum C1+C3 during background conditions with fresh water fracture, b) Cross-polarized sum C1+C3 during the natural gradient saline tracer test, c) Co-polarized sum P1+P3 during background conditions, and d) Co-polarized sum P1+P3 during the natural gradient saline tracer test.

Discussion and Conclusions

The objective of this study is to examine if cross-polarized GPR signals can image channeling along a discrete fracture. Observations made by the numerical models are in agreement with the expected theoretical responses when considering the subsurface model being the superposition of horizontal planar interfaces and a cylinder. The horizontal planar interfaces do not depolarize the incident waveflied and therefore the reflected signal does not contain cross-polarized components. A cylindrical channel oriented parallel or orthogonal to the incident wavefield is also not expected to result in depolarized components. When the cylindrical channel is oriented obliquely to the incident wavefiled depolarization results in scattered energy along the cross-polarized components. Therefore, when using GPR to image fractures in a natural environment it is very likely that the cross-polarized components contain information about channels oriented obliquely to the survey lines. Modeling also confirms that acquisition of two orthogonal polarizations is needed to fully image a horizontal fracture containing channels. When the channel is oriented parallel or orthogonal to the survey line, summation of the co-polarized data captures all scattered energy. When the channel is oriented oblique to the survey line, vector summation of the co- and cross-polarized components results in an accurate representation of the scattered energy. Field GPR monitoring of a natural gradient tracer test showed for the first time the utility of cross-polarized signal components for imaging flow channeling. GPR cross-polarized components are shown to contain information about fracture channels and therefore should be recorded for accurate subsurface imaging.

Acknowledgements

This research was supported by the US Department of Energy Environmental Remediation Sciences Program 07-358509 and the US Department of Energy Geothermal Technologies Program DE-EE0002767. Instrumentation was funded by the National Science Foundation EAR/IF-0345445. We would like to thank the Miner Institute, Adam Hawkins and Blair Schneider for supporting field activities.

References

Davis, J. L., and A. P. Annan (1989), Ground penetrating radar for high-resolution mapping of soil and rock stratigraphy: Geophysical Prospecting, 37, 531–551.

Day-Lewis, F.D., J.W. Lane, 762 J.M. Harris, and S.M. Gorelick (2003), Time-lapse imaging of saline-tracer transport in a fractured rock using difference-attenuation radar tomography, Water Resour. Res., 39, 1290, doi: 10.1029/2002WR001722.

Deparis, J., and S. Garambois (2009), On the use of dispersive APVO GPR curves for thin bed properties estimation: Theory and application to fracture characterization, Geophysics, 780 74 (1), J1-J12, doi : 10.1190/1.3008545.

Dorn, C., N. Linde, T. Le Borgne, O. Bour, and L. Baron (2011), Single-hole GPR reflection imaging of solute transport in a granitic aquifer, *Geophys. Res. Lett., 38*, L08401, doi:770 10.1029/2011GL047152.

Dorn, C., N. Linde, T. Le Borgne, O. Bour, *and* M. Klepikova *(*2012*)*, Inferring transport characteristics in a fractured rock aquifer by combining single-hole ground-penetrating radar reflection monitoring and tracer test data, Water Resour. Res., 48, W11521, doi:10.1029/2011WR011739.

Lehmann, F., Boerner, D. E., Holliger, K., and Green, A. G. (2000), Multicomponent georadar data: Some important implications for data acquisition and processing: Geophysics, v. 65, p. 1542.

Giannopoulos, A. (2005), Modelling ground penetrating radar by GprMax: Construction and Building Materials, v. 19, no. 10, p. 755-762.

Radzevicius, S. J., and Daniels, J. J. (2000), Ground penetrating radar polarization and scattering from cylinders: Journal of Applied Geophysics, v. 45, no. 2, p. 111-125.

Roberts, R. L., and Daniels, J. J. (1996), Analysis of GPR Polarization Phenomena: Journal of Environmental and Engineering Geophysics, v. 1, p. 139.

Sato, M., and Miwa, T. (2000), Polarimetric borehole radar system for fracture measurement: Subsurface Sensing Technologies and Applications, v. 1, no. 1, p. 161-175.

Talley, J., G.S. Baker, M.W. Becker, and N. Beyrle (2005), Four dimensional mapping of tracer channelization in subhorizontal bedrock fractures using surface ground penetrating radar, Geophys. Res. Lett., 32, L04401, doi: 10.1029/2004GL021974.

Tsang, C.F., and I. Neretnieks (1998), Flow channeling in heterogeneous fractured rocks, Rev. Geophys., 36, 275-298.

Tsoflias, G. P., T. Halihan, and J. M. Sharp Jr. (2001), Monitoring pumping test response in a fractured aquifer using ground penetrating radar: Water Resour. Res., 37, 1221–1229.

Tsoflias, G. P., J. P. Van Gestel, P. Stoffa, D. Blankenship, and M. Sen (2004), Vertical fracture detection by exploiting the polarization properties of GPR signal, Geophysics, 69, 803–810.

Tsoflias, G.P., and M.W. Becker (2008), Ground-penetrating-radar response to fracture-fluid salinity: Why lower frequencies are favorable for resolving salinity changes, Geophysics, 73 (5), J25-J30, doi: 10.1190/1.2957893**.**

Tsoflias G. P., Baker M., and M. Becker (2012), Field GPR monitoring of flow channeling in fractured rock: Abstract NS51B-1834, Fall AGU Meeting, San Francisco, Calif., December 3-7, 2012.

Appendix F

Tsoflias, G. P., M. Baker, and M. W. Becker (2013), Imaging fracture anisotropic flow channeling using GPR signal amplitude and phase, in *SEG Technical Program Expanded Abstracts*, edited, pp. 4428-4433.

Imaging fracture anisotropic flow channeling using GPR signal amplitude and phase

Georgios Tsoflias and Matthew Baker, The University of Kansas; Matthew Becker, California State University Long Beach*

Summary

Flow in fractured rocks is highly heterogeneous and occurs along preferred pathways referred as flow channels. Conventional borehole hydraulic tests do not capture the heterogeneous flow properties of fractured rock. We present a field investigation of ground-penetrating radar (GPR) imaging of anisotropic channeled flow along a discrete fracture. Dipole-flow tests conducted in a five-spot well field allow control over the orientation of the hydraulic gradient. Multi-polarization, 3D GPR imaging is used in time-lapse mode to monitor dipole-flow saline tracer tests. The presence of saline tracer in the fracture results in reflected GPR signal amplitude increase and phase decrease relative to fresh water. Tracer flow channeling is assessed by comparing GPR imaging of the fracture containing fresh water (background) with east-west (E-W) and north-south (N-S) oriented dipole tracer tests. GPR signal amplitude and phase changes reveal that the E-W dipole results in a direct and narrow channeled flow field of least resistance between boreholes. The N-S dipole causes a wider surface area of the fracture to be swept by the tracer suggesting poorer hydraulic connection than the E-W path. GPR imaging results of flow channeling are supported by hydraulic tracer tests conducted at the site. This work presents for the first time a) the use of GPR phase for imaging the spatial distribution of saline tracer in a fracture, and b) imaging in the field flow channeling changes in response to hydraulic gradient orientation changes.

Introduction

Fractures control the flow of fluids in rocks with important implications for groundwater resources, contaminant transport, geothermal resources, sequestration of carbon dioxide, and the development of unconventional hydrocarbon resources. However, fractured rocks exhibit heterogeneous hydraulic properties that are difficult to characterize using conventional hydraulic testing methods (e.g. Becker and Shapiro, 2000; 2003). Flow channeling caused by fracture aperture variability is known to result in preferential pathways of flow and transport (Moreno and Tsang, 1994; Tsang and Neretnieks, 1998).

GPR has been shown to be an effective method for imaging fractures (e.g. Davis and Annan, 1989; Grasmueck, 1996; Grégoire et al., 2003; Deparis and Garambois, 2009; Tsoflias et al., 2004) and determining fluid content (Lane et al., 2000; Tsoflias et al., 2001). Time-lapse GPR imaging has been used to monitor saline tracer movement in fractured rock and identify pathways of preferential flow (e.g. Day-Lewis et al., 2003; Dorn et al., 2011; 2012; Talley et al., 2005). Tsoflias and Becker (2008) showed characteristic GPR signal amplitude increase and phase decrease associated with increasing electrical conductivity of water in a discrete fracture, and they exploited GPR amplitude breakthrough to estimate fracture hydraulic properties (Becker and Tsoflias, 2010).

The work presented here exploits the amplitude and phase response of reflected GPR signals to image flow channeling at a discrete fracture under variable hydraulic gradient orientation.

Methods

GPR field experiments were conducted at the Altona Flat Rock site, 15 km northwest of Plattsburgh, NewYork, in the William Miner Experimental Forest. The site is instrumented with five boreholes that are used to conduct dipole flow tracer tests (Fig. 1a). The dipole tests were established by re-circulation of saline traced formation water between injection and pumping boreholes through a hydraulically conductive subhorizontal fracture 7.6 m below ground surface (Fig 1b).

Three-dimensional, multi-polarization GPR data were acquired under the following hydrologic conditions:

a) Background natural gradient with fresh water in the fracture (9 mS/m)
b) E-W oriented dipole flow tracer test and,
c) N-S oriented dipole flow tracer test.

Each dipole tracer test re-circulated approximately 400 mS/m electrical conductivity water through the fracture. The 3D GPR grids covered a 100 m^2 area at 0.25 m x 0.5 m trace spacing. Radar data were acquired at 50 MHz and 100 MHz frequencies using broadside and cross-polarized dipole antenna pairs oriented parallel and orthogonal to the survey grid lines. A prior investigation at the site (Tsoflias et al., 2011) determined that multi-polarization acquisition is necessary in order to accurately image channeling along the fracture plane (Fig 2).

GPR data processing consisted of instrument calibration between the two radar systems, temporal calibration for instrument response drift between time-lapse surveys, time-zero correction, frequency filtering and migration. After

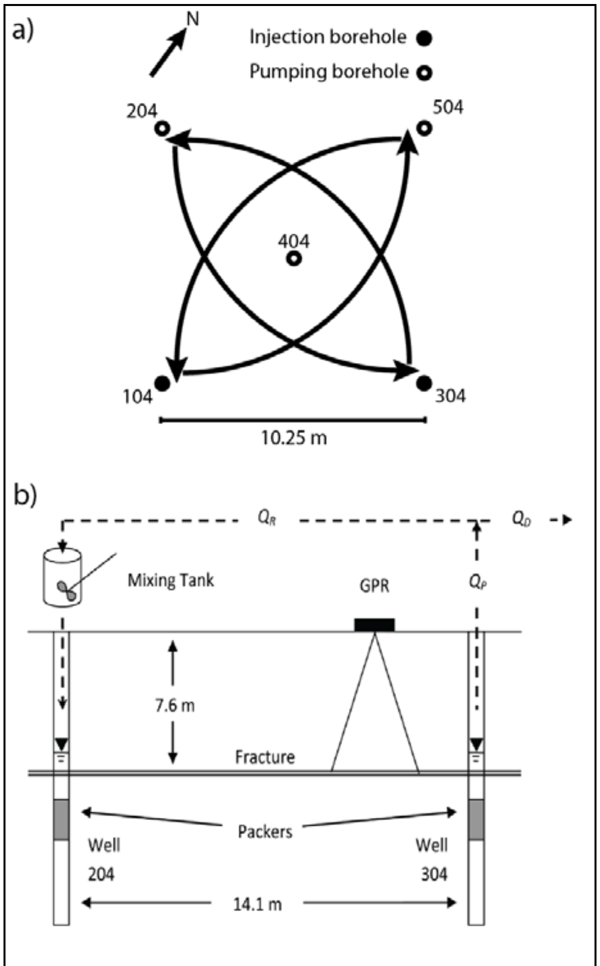

Figure 1: a) Dipole flow schematic and b) tracer test experimental set-up.

calibration and processing, individual broadside polarization data were summed to form pseudoscalar radar volumes (Lehmann et al., 2000) and to reduce dipole antenna directionality effects on fracture channel imaging (Tsoflias et al., 2011).

Results

Time-lapse imaging mode assesses changes in radar reflectivity (i.e. signal amplitude and phase) associated with changes in fluid electrical conductivity while fracture aperture and host rock properties remain unchanged. Differencing time-lapse data allows us to isolate the effect of the property that is changing over time, i.e. tracer concentration and flow orientation, and to monitor paths of tracer transport, i.e. flow channeling.

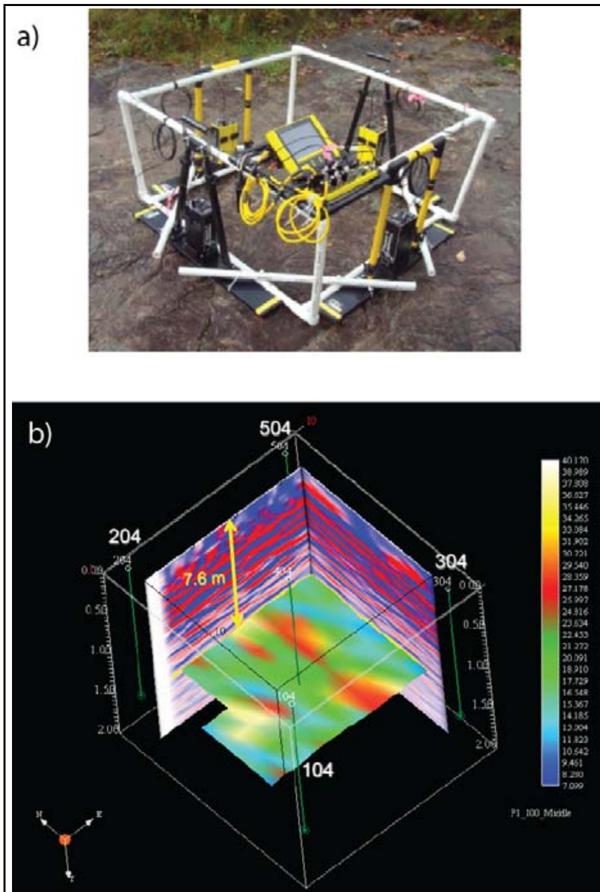

Figure 2: a) 100 MHz multi-polarization acquisition GPR system. b) 3D view of GPR data volume.

Reflection coefficient analytical models of varying fracture aperture and water electrical conductivity indicate that for any given aperture an increase in water electrical conductivity would result in an increase of reflected signal amplitude and a decrease of the signal phase (Fig 3).

Figure 4 displays fracture reflection amplitude and phase for background conditions and dipole tracer tests in E-W and N-S orientations. Increasing negative amplitudes (blue color) of the background (fresh water) grid are interpreted to correspond to regions of greater aperture along the fracture plane. The phase response of the fresh water filled fracture exhibits relatively small change to changing aperture as predicted by the analytical model in figure 3b. GPR signal amplitude is expected to increase as saline tracer concentration increases (Fig 3a). GPR amplitudes in figure 4 delineate a narrow and direct flow channel in the E-W (wells 204-304) dipole test which agrees with the good hydraulic connectivity between wells 204 and 304 that has been observed in hydraulic tests. The N-S (104-

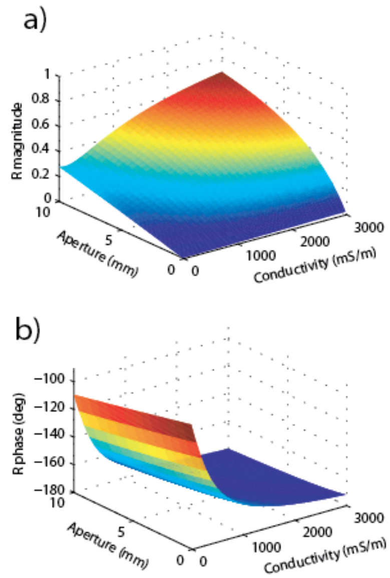

Figure 3: Analytical modles of reflection coefficient a) magnitude and b) phase as a function of fracture aperture and water electrical conductivity for a 100 MHz frequency signal.

504) dipole tracer test reveals wider, more tortuous flow channeling between wells 104 and 504 which is in agreement with poor hydraulic connectivity observed between the two wells.

Changes observed in the GPR phase data (Fig. 4) are analogous to the changes observed in the amplitude data. GPR signal amplitude is expected to increase with increasing water salinity, whereas phase is expected to decrease. The tracer transport paths detected by GPR phase are in good agreement with the flow channels identified by the amplitude data. It should be noted that signal phase is sensitive to small changes in water electrical conductivity compared to amplitude (Fig 3) therefore, the flow channels defined by phase changes are in general broader than the regions of amplitude change.

The effect of saline tracer circulation through the fracture plane is best illustrated by differencing the background amplitude and phase data from the E-W and N-S dipole flow data (Fig. 5). By subtracting the background fresh water data we are effectively removing the effect of the fracture aperture which allows us to delineate the flow paths of the saline tracer. GPR signal amplitude and phase difference data show that the E-W dipole results in a direct and narrow channeled flow field between boreholes 304 and 204. The N-S dipole causes a wider surface area of the fracture to be swept by the tracer suggesting poorer hydraulic connection than the E-W path.

Conclusions

Ground penetrating radar imaging of a discrete fracture shows that reflected signal amplitude and phase changes can be used to monitor saline tracer flow and to delineate flow channeling. This work demonstrates at the field scale that flow channeling can be anisotropic and strongly dependent on the orientation of the hydraulic gradient. Changes in flow direction can cause the fracture channels to vary from narrow well connected conduits of rapid flow to poorly connected, broad and tortuous paths. The same fracture is shown to exhibit different flow properties as the orientation of the hydraulic gradient changes.

Acknowledgements

DOE Environmental Remediation Sciences Prog. 07-358509; US DOE Geothermal Technologies Prog. DE-EE0002767; NSF EAR/IF-0345445; Miner Institute; Chris Perll, Adam Hawkins, Blair Schneider.

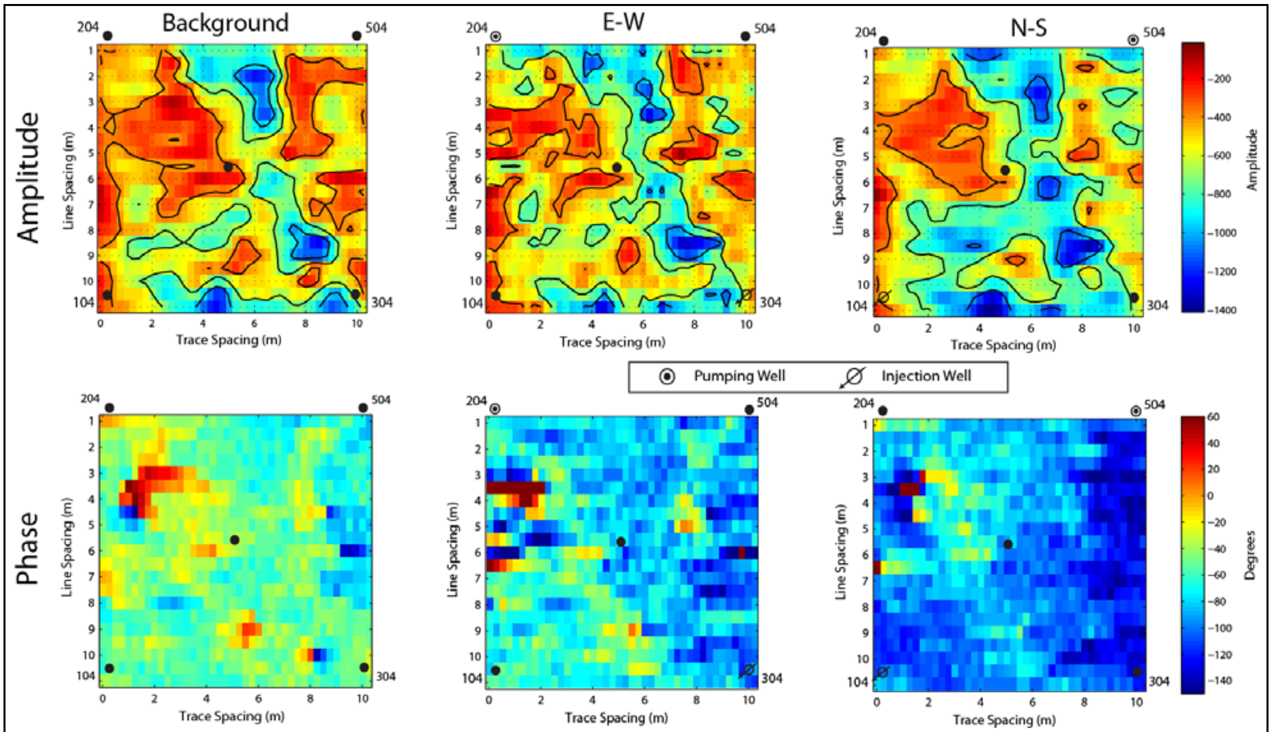

Figure 4: Fracture reflector amplitude and phase under background fresh water and 400 mS/m dipole tracer tests in E-W and N-S orientations. GPR data frequency is 100 MHz.

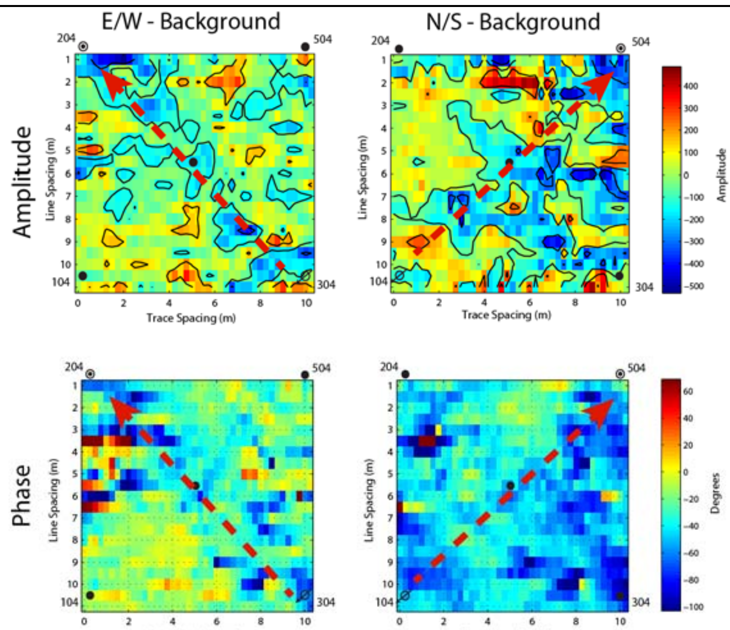

Figure 5: Amplitude and phase difference from backround for the E-W and N-S dipole tracer tests. Arrows identify the direction of the diploe flow test. GPR data frequency is 100 MHz.

References

Becker, M.W., and A.M. Shapiro (2003), Interpreting tracer breakthrough tailing from different forced-gradient tracer experiment configurations in fractured bedrock, Water Resour. Res., 39, 1024, doi: 10.1029/2001WR001190.

Becker, M.W., and A.M. Shapiro (2000), Tracer transport in fractured crystalline rock: Evidence of nondiffusive breakthrough tailing, Water Resour. Res., 36, 1677-1686, doi: 746 10.1029/2000WR900080.

Becker, M.W., and G.P. Tsoflias (2010), Comparing flux-averaged and resident concentration in a fractured bedrock using ground penetrating radar data, Water Resour. Res., 46, W09518, doi: 10.1029/2009WR008260.

Davis, J. L., and A. P. Annan (1989), Ground penetrating radar for high-resolution mapping of soil and rock stratigraphy: Geophysical Prospecting, 37, 531–551.

Day-Lewis, F.D., J.W. Lane, 762 J.M. Harris, and S.M. Gorelick (2003), Time-lapse imaging of saline-tracer transport in a fractured rock using difference-attenuation radar tomography, Water Resour. Res., 39, 1290, doi: 10.1029/2002WR001722.

Deparis, J., and S. Garambois (2009), On the use of dispersive APVO GPR curves for thin bed properties estimation: Theory and application to fracture characterization, Geophysics, 780 74 (1), J1-J12, doi : 10.1190/1.3008545.

Dorn, C., N. Linde, T. Le Borgne, O. Bour, and L. Baron (2011), Single-hole GPR reflection imaging of solute transport in a granitic aquifer, *Geophys. Res. Lett., 38*, L08401, doi:770 10.1029/2011GL047152.

Dorn, C., N. Linde, T. Le Borgne, O. Bour, *and* M. Klepikova *(*2012*),* Inferring transport characteristics in a fractured rock aquifer by combining single-hole ground-penetrating radar reflection monitoring and tracer test data, Water Resour. Res., 48, *W11521, doi:10.1029/2011WR011739.*

Grasmueck, M. (1996), 3-D ground-penetrating radar applied to fracture imaging in gneiss: Geophysics, 61, 1050–1064.

Grégoire, C., L. Halleux, and V. Lukas (2003), GPR abilities for the detection and characterization of open fractures in a salt mine: Near Surface Geophysics, 1, 139–147.

Lane, J.W. Jr., M. L. Buursing, F. P. Haeni, and R. J. Versteeg (2000), Evaluation of ground-penetrating radar to detect free-phase hydrocarbons in fractured rocks - Results of numerical modeling and physical experiments: GroundWater, 38, 929–938.

Lehmann, F., D.E. Boerner, K. Holliger, and A.G. Green (2000), Multicomponent georadar data: Some important implications for data acquisition and processing, Geophysics, 65, 1542-1552.

Moreno, L., and C.F. Tsang (1994), Flow channeling in strongly heterogeneous porous media: A numerical study, Water Resour. Res., 30 (5), 1421-140, doi: 10.1029/93WR02978.

Talley, J., G.S. Baker, M.W. Becker, and N. Beyrle (2005), Four dimensional mapping of tracer channelization in subhorizontal bedrock fractures using surface ground penetrating radar, Geophys. Res. Lett., 32, L04401, doi: 10.1029/2004GL021974.

Tsang, C.F., and I. Neretnieks (1998), Flow channeling in heterogeneous fractured rocks, Rev. Geophys., 36, 275-298.

Tsoflias, G. P., T. Halihan, and J. M. Sharp Jr. (2001), Monitoring pumping test response in a fractured aquifer using ground penetrating radar: Water Resour. Res., 37, 1221–1229.

Tsoflias, G. P., J. P. Van Gestel, P. Stoffa, D. Blankenship, and M. Sen (2004), Vertical fracture detection by exploiting the polarization properties of GPR signal, Geophysics, 69, 803–810.

Tsoflias, G.P., and M.W. Becker (2008), Ground-penetrating-radar response to fracture-fluid salinity: Why lower frequencies are favorable for resolving salinity changes, Geophysics, 73 (5), J25-J30, doi: 10.1190/1.2957893**.**

Tsoflias G. P., Baker M. and M. W. Becker (2011), Assessing GPR signal polarization for 3D imaging of fracture flow Channels, Abstract NS41A-07, Fall AGU Meeting, San Francisco, Calif., December 5-9, 2011.

Appendix G

M. W. Becker (2013, Homework Assignment, GEOL 477/577, *Physical Hydrogeology*, Department of Geology, California State University Long Beach.

Hydrogeology Homework #9: Solutions

1. A pump test was performed in a single isolated fracture in a sandstone bedrock. Well 404 was pumped at 4.2 L/min and drawdown was observed at well 304 (7 m away) , well 104 (7 m away) and well 492 (31 m away). Data are provided in the spreadsheet on Beachboard.

a. Plot all three datasets in Cooper-Jacob Format

b. Use a trendline to find T and S for each of the three wells

c. Using the T and S estimates, calculate u values to evaluate the validity of the Cooper-Jacob approximation.

The normalized plots of drawdown (s/Q) versus time (t/r2) are:

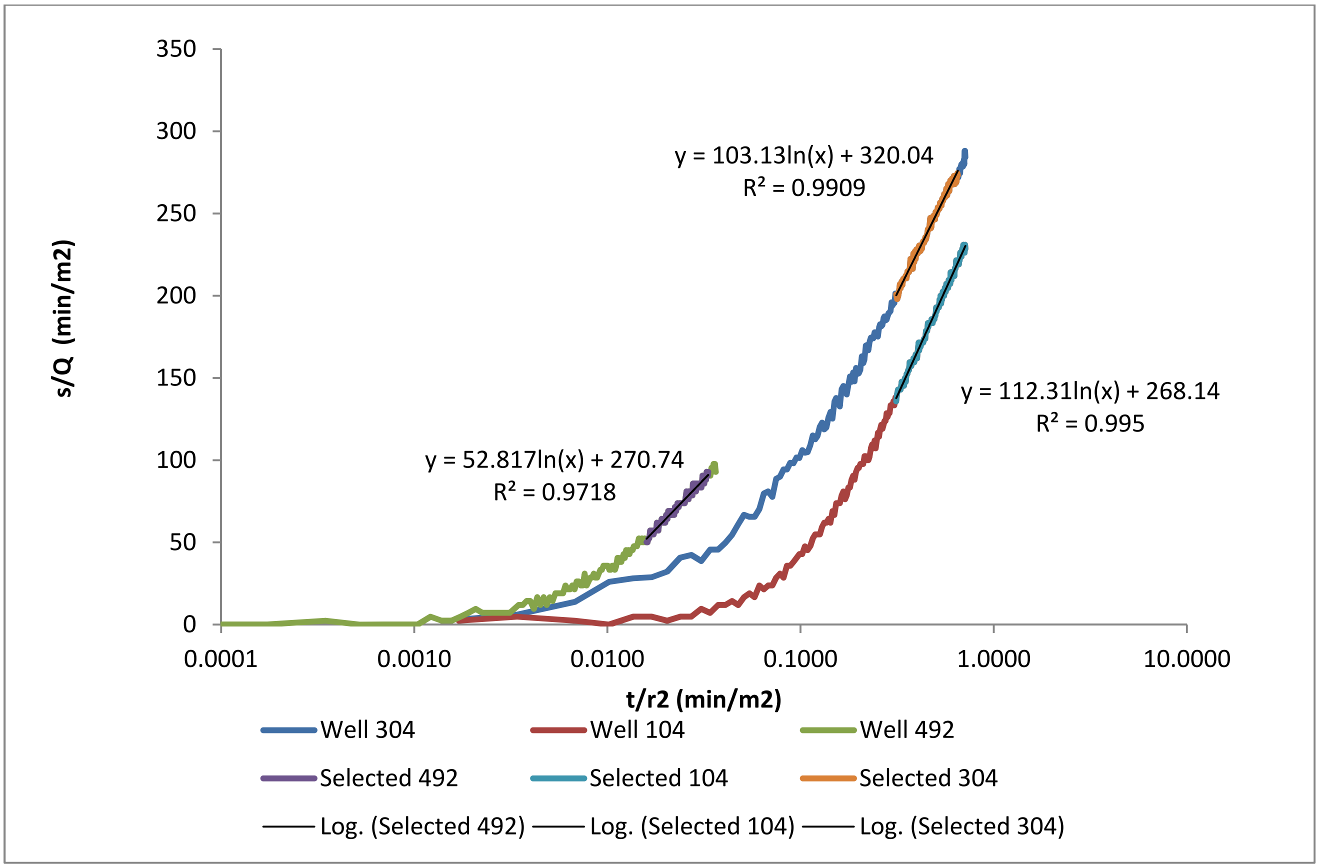

Checking for the u value, which should be u<0.1 for <5% error Cooper Jacob, calcuation, where $u = r^2S/4Tt$... the straight line portions were taken after about 30 minutes of drawdown.

Well	r (m)	Slope	Intercept	T (m2/min)	S	t (min)	u (30min)	T (ft2/min)
Well 492	31	52.82	270.74	1.5E-03	2.0E-05	19.22	0.11	1.6E-02
Well 304	7	103.13	320.04	7.7E-04	7.8E-05	9.8	0.04	8.3E-03
Well 104	7	112.31	268.14	7.1E-04	1.5E-04	9.8	0.08	7.6E-03

So the Cooper Jacob approximation is decent after about 30 minutes of drawdown, but some error (>5%) might be expected in Well 492.

After plotting s/Q vs. t/r^2 and solving for slope.

$$\frac{s}{Q} = \frac{1}{4\pi T} \ln\left(t/r^2\right) + \frac{1}{4\pi T} \ln\left(\frac{2.25\,T}{S}\right)$$

$$y = m \quad \ln(x) \quad + \quad b$$

for well 492 $\quad m = 52.8 \quad b = 270.7$

$$m = \frac{1}{4\pi T} \qquad T = \frac{1}{4\pi m} = \frac{1}{4\pi(52.8)} = \boxed{1.5 \cdot 10^{-3}\ m^2/min}$$

* Note units must be consistent – i.e. m & min on the plot.

$$S = 2.25\,T \exp\left(-4\pi T b\right)$$

$$= 2.25 \cdot (1.5 \cdot 10^{-3}) \exp\left[-4\pi(1.5 \cdot 10^{-3})(270.7)\right]$$

$$= \boxed{2.0 \cdot 10^{-5}}$$ – no units on S.

repeating calculations gives attached table for remaining wells